

Geometric theory for multi-bump, self-similar, blowup solutions of the cubic nonlinear Schrödinger equation

Vivi Rottschäfer¹ and Tasso J Kaper²

¹ Mathematical Institute, Leiden University, PO Box 9512, 2300 RA Leiden, The Netherlands

² Department of Mathematics and Centre for BioDynamics, Boston University,
111 Cummington Street, Boston, MA 02215, USA

Received 30 August 2002, in final form 4 February 2003

Published 14 March 2003

Online at stacks.iop.org/Non/16/929

Recommended by W J Zakrzewski

Abstract

We establish the existence and local uniqueness of two classes of multi-bump, self-similar, blowup solutions for the cubic nonlinear Schrödinger equation close to the critical dimension $d = 2$. Our results for one class of orbits build on the earlier discovery of these orbits via numerical simulation and via asymptotic analysis, providing a proof of their existence. The second class of multi-bump orbits is new. These multi-bump orbits, many of which are thought to be unstable, appear to serve as guides for how different types of initially nonmonotone data might blow up.

These self-similar solutions are governed by a nonlinear, nonautonomous ordinary differential equation (ODE); and, when linearized, this ODE exhibits hyperbolic behaviour near the origin and elliptic behaviour asymptotically. In between, the behaviour changes type; this region is called the midrange. For the solutions of the full ODE that we construct, all but one of the bumps—the exception being the central bump at the origin—lie in the midrange. The main steps in the proof involve (i) tracking a pair of manifolds of solutions of the governing ODE that satisfy the conditions at the origin and the asymptotic conditions, respectively, to a common point in the midrange, and (ii) showing that these intersect transversally. Geometric singular perturbation theory, adiabatic Melnikov theory, and the exchange lemma are used to analyse the dynamics in the midrange.

Mathematics Subject Classification: 35Q55

1. Introduction

The cubic nonlinear Schrödinger equation,

$$i \frac{\partial \Phi}{\partial t} + \Delta \Phi + |\Phi|^2 \Phi = 0, \quad (1.1)$$

is a Hamiltonian partial differential equation whose solutions lie on the level sets of the energy function,

$$H(\Phi) = \int [|\nabla\Phi|^2 - \frac{1}{2}|\Phi|^4] dx \quad (1.2)$$

and have conserved mass,

$$M = \int_0^\infty |\Phi|^2 dx. \quad (1.3)$$

Its dynamics are extremely rich both in one space dimension and in higher space dimensions (see, e.g., [5, 36, 37]). In addition, it arises as the governing equation in many scientific problems. See [6, 12, 15, 31, 37] for some of the examples in nonlinear optics and plasma physics.

Numerical simulations show that there exist solutions of (1.1) in dimensions $2 \leq d < 4$, such as those for which the Hamiltonian (1.2) of the initial condition is negative, that are singular in finite time, i.e. the solutions become infinite at a single point (see [24–28]). The nonlinearity dominates the dispersive term. Hence, when the initial conditions are large enough in a suitable norm, a spatial contraction of the wave packet takes place, and the amplitude grows, resulting in the blowup of the wave amplitude. In nonlinear optics, this singularity corresponds to an extreme increase of the field amplitude due to self-focusing; in plasma physics, this phenomenon is called collapse.

The most thoroughly studied blowup solutions have one peak (or bump) centred at the origin. The moduli of these solutions are monotone, and they are close, to leading order, to the ground state solution of the classical equation, written here for $d = 2$:

$$R_{xx} + \frac{1}{x}R_x - R + R^3 = 0. \quad (1.4)$$

Most interestingly, for $2 < d < 4$, these solutions are symmetric and asymptotically self-similar. They have been analysed using the method of dynamical rescaling (see [24, 27]). This method exploits the asymptotically self-similar behaviour of the solutions. Here, space, time, and Φ are scaled by factors of a suitably chosen norm of the solutions, denoted by $L(t)$, which blows up at the singularity,

$$\xi \equiv \frac{|x|}{L(t)}, \quad \tau \equiv \int_0^t \frac{1}{L^2(s)} ds, \quad u(\xi, \tau) = L(t)\Phi(x, t). \quad (1.5)$$

The corresponding norm of the rescaled solution u remains constant in time; and, as a consequence, the rescaled problem is no longer singular. The rescaled solution u satisfies

$$iu_\tau + u_{\xi\xi} + \frac{d-1}{\xi}u_\xi + |u|^2u + ia(\tau)(\xi u)_\xi = 0,$$

where

$$a = -L \frac{dL}{dt} = -\frac{1}{L} \frac{dL}{d\tau}.$$

Looking for radially symmetric, blowup solutions of the self-similar type corresponds to setting a to be a constant.

In addition, for $2 < d < 4$, it is found that the numerical solution becomes stationary (a fixed profile) up to a linearly increasing phase in τ [37]. This suggests looking for u in the form $u = e^{ic\tau}Q(\xi)$ for some c that depends on the solution. Scaling τ with $1/c$ leads to the following equation for Q :

$$Q_{\xi\xi} + \frac{(d-1)}{\xi}Q_\xi - Q + ia(\xi Q)_\xi + |Q|^2Q = 0. \quad (1.6)$$

Moreover, given the initial and asymptotic conditions for Φ , namely that $\Phi(x, 0) = \Phi_0(x)$ and that $|\Phi|$ vanishes as $|x| \rightarrow \infty$, respectively, the initial and asymptotic conditions for Q are, respectively,

$$Q_\xi(0) = 0, \quad \text{Im}Q(0) = 0, \quad (1.7)$$

$$|Q(\xi)| \rightarrow 0 \quad \text{as } \xi \rightarrow \infty. \quad (1.8)$$

Finally, Q must satisfy the global constraint

$$H(Q) = 0, \quad (1.9)$$

since the Hamiltonian H must be finite (after the rescaling).

The parameter a plays the role of a nonlinear eigenvalue. For each sufficiently small value of a , numerical simulations show that there is a unique value of $d = d(a)$ at which the single-bump, self-similar, blowup solution exists. These simulation results have been confirmed by asymptotic analysis, which shows that $d(a) = 2 + \mathcal{O}(e^{-\pi/a})$, as $a \rightarrow 0$ (see [25–27]). In addition, for dimensions d that are exponentially close to 2, $d = 2 + \mathcal{O}(e^{-\pi/a})$, as well as for dimensions d that satisfy $|d-2| \leq \mathcal{O}(a^\ell)$ for $\ell > 0$, the existence and local uniqueness of these single-bump solutions has been shown using invariant manifold theory and other techniques from dynamical systems theory, see [23] and [35], respectively.

Recently, numerical simulations and asymptotic analysis of (1.1) in dimensions $2 < d < 4$ have shown that there also exist self-similar, blowup solutions that need not be monotone, see [3] and [2], respectively. A doubly countable set of multi-bump solutions $Q_{K,J}(\xi)$ with $(K, J) \in (0, 1, 2, \dots) \times (0, 1, 2, \dots)$ is found, where—for each a sufficiently small—the moduli $|Q_{K,J}|$ have $K+J$ local maxima. Moreover, these are each observed for unique values of d such that $d \rightarrow 2^+$ as $a \rightarrow 0$. The solutions satisfy two asymptotic properties as $d \rightarrow 2^+$. First, the $|Q_{K,J}(\xi)|$ converge to solutions $R_K(\xi)$ on $\mathcal{O}(1)$ intervals starting at $\xi = 0$ as $a \rightarrow 0$ and $d \rightarrow 2$, where R_K , $K = 0, 1, 2, \dots$, is defined as the solution of equation (1.4) that has $K-1$ zeros and K turning points for $\xi \geq 0$. See [29] for an analysis of (1.4); we note that $R_0(\xi)$ vanishes identically everywhere and that $R_1(\xi)$ is the ground state solution to which $|Q_{1,0}|$ converges uniformly. Second, for each multi-bump solution and a small, $|Q_{K,J}|$ has J local maxima in the range $\xi = \mathcal{O}(1/a)$, just to the left of $\xi = 2/a$, which is the point where the linearization of (1.6) has a turning point. Hence, in the limit $a \rightarrow 0^+$, all of these J bumps are created at $\xi = \infty$, as observed in [2].

The solutions with $K = 0$ ($J = 1, 2, 3$) and $K = 1$ ($J = 0, 1, 2$) obtained via numerical simulations are presented in [3]. To our knowledge, these are the only solutions that have been found so far numerically. Figure 1, which is a reproduction of figure 1.2 from [2], shows the multi-bump solutions for $K = 1$ and $J = 0, 1, 2$.

In this paper, we establish the existence and local uniqueness of two classes of n -bump solutions for each fixed $d > 2$ such that $|d-2| \leq \mathcal{O}(a^\ell)$, with $0 < a \ll 1$ and $\ell > d+1$, where $n = K+J$, $K = 1$, and $J = 0, 1, 2, 3, \dots$, in terms of the notation of [2]. The moduli of these solutions have a maximum at $\xi = 0$. For some interval of values of $\xi > 0$, $|Q|$ decreases monotonically to become exponentially small. Then, in the interval $\xi \in [\xi_b, \xi_{\max}]$, which lies in the so-called midrange, $|Q|$ has $n-1$ local maxima, which lie just to the left of $\xi = 2/a$ and which are $\mathcal{O}(\log(1/a))$ apart. Here, $\xi_b = k_b \log(1/a)$ for some positive constant k_b , and $\xi_{\max} = (2 - \sqrt{a})/a$. The solutions of the two types are different from one another and are distinguished by the value of $|Q|$ at $\xi = \xi_{\max}$. For solutions of type L, the modulus $|Q|$ is exponentially small at $\xi = \xi_{\max}$; whereas, $|Q|$ is strictly $\mathcal{O}(a^{3/8})$ at $\xi = \xi_{\max}$ for solutions of type R. The solutions of type L are the solutions $Q_{1,J}$ found in [2], whereas the solutions of type R have, to our knowledge, not been found either in numerical simulations or in asymptotic analysis so far. Finally, the n -bump solutions of type L lie exponentially close to each other.

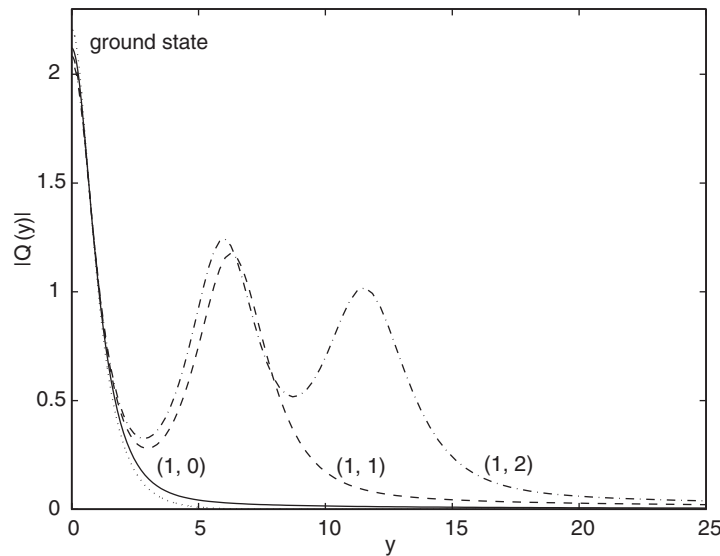


Figure 1. The functions $Q_{K,J}(\xi)$ for $(K, J) = (1, 0)$, $(1, 1)$ and $(1, 2)$ when $d = 2.01$. This is a reproduction of figure 1.2 in [2] (reproduced with the permission of the author).

Remark 1.1. Choosing a non-integer dimension is equivalent to taking $d = 2$ and the power of the nonlinear term equal to 2σ for some σ such that $\frac{1}{2} \leq \sigma < 1$.

Remark 1.2. We refer the reader to [2] for a discussion of the observations that some of the multi-bump solutions that have multiple local maxima for d near 2 appear to be monotone instead when continued to dimension $d = 3$.

2. Statement of the main result and the strategy for its proof

In this section, we state the main theorem—the content of which has been described at the end of the previous section—and the strategy we employ to prove it. The main result of this paper is the following theorem.

Theorem 2.1. *For each $a > 0$ sufficiently small, there exists an $n_0(a)$ such that, if $2 \leq n \leq n_0(a)$, then with $d - 2 = \mathcal{O}(a^\ell)$ (nonstrict) for any $\ell > d + 1$ there exist $4(n - 1)$ locally unique n -bump solutions of the type studied here of the problem given by equation (1.6) and the initial conditions, boundary conditions, and global constraint (1.7), (1.8), and (1.9), respectively. These solutions consist of n local maxima each on $0 \leq \xi < \xi_{\max}$, where $\xi_{\max} = (2 - \sqrt{a})/a$, one of which is at $\xi = 0$ and the other $n - 1$ of which are strictly $\mathcal{O}(\log(1/a))$ apart. Of the $4(n - 1)$ locally unique n -bump solutions, $2n - 1$ are characterized by the property that $|Q(\xi_{\max})|$ is exponentially small, and they are said to be of type L. The other $2n - 3$, said to be of type R, instead satisfy $|Q(\xi_{\max})| = ca^{3/8} - \tilde{c}a^{5/8}$, for some positive constant c and a positive function $\tilde{c} = \tilde{c}(c)$; and, the n th local maximum occurs near ξ_{\max} , where $|Q(\xi_{\max})| = \sqrt{2}a^{1/4}(1 - \frac{1}{8}\sqrt{a}) + \text{hot}$. Moreover, there exists a 1-bump solution that has one local maximum at $\xi = 0$ and that is monotonically decreasing.*

Remark 2.1. It will be shown that $n_0(a)$ increases as a decreases. Also, the restriction $\ell > d + 1$ is derived in the proof of lemma 8.2 below, and the function $\tilde{c}(c)$ is given in lemma 7.2.

The stated problem, equation (1.6) with the initial and boundary conditions and the global constraint, is not strictly a boundary value problem because of the global constraint (1.9). This constraint may be replaced by a local asymptotic condition as $\xi \rightarrow \infty$. Due to the boundary condition (1.8), it follows that for large ξ , the behaviour of the solutions is described by the linear part of equation (1.6):

$$Q_{\xi\xi} + \frac{(d-1)}{\xi} Q_{\xi} - Q + ia(\xi Q)_{\xi} = 0. \quad (2.1)$$

For this equation, there exists a pair of linearly independent solutions for large ξ that are given by

$$Q_1 \sim \xi^{-1-i/a}, \quad Q_2 \sim \xi^{-(d-1-i/a)} e^{-ia(\xi^2/2)} \quad (2.2)$$

(see [27, 36]). Since Q_2 does not satisfy (1.9) (H is infinite), the limiting profile of a solution for large ξ must be a multiple of Q_1 . Thus, a necessary condition for the solution to satisfy (1.9) is that it is a multiple of Q_1 . It follows from an argument in [26] that this is also sufficient. There, it is shown that if H is finite then it is zero. The asymptotic expressions for Q_1 and its derivative imply that (1.9) is satisfied if and only if

$$\left| \xi Q_{\xi} + \left(1 + \frac{i}{a}\right) Q \right| \rightarrow 0 \quad \text{as } \xi \rightarrow \infty. \quad (2.3)$$

Therefore, we may replace (1.9) by (2.3) (see [3]). Moreover, from the fact that Q_1 decays at ∞ , it follows that the boundary condition (1.8) is satisfied. This implies that (1.8) can be omitted. Therefore, we study equation (1.6) with the conditions (1.7) and (2.3).

The analysis of (1.6) is carried out by decomposing Q into amplitude and phase,

$$Q(\xi) = A(\xi) \exp \left[i \int_0^{\xi} \psi(x) dx \right], \quad B(\xi) = \frac{A_{\xi}}{A}. \quad (2.4)$$

Here, A is the amplitude, B its logarithmic derivative, and ψ is the gradient of the phase. Then, (1.6) reduces to

$$\begin{aligned} A_{\xi} &= AB, \\ B_{\xi} &= \frac{(1-d)B}{\xi} + \psi^2 - B^2 - A^2 + 1 + a\xi\psi, \\ \psi_{\xi} &= \frac{(1-d)\psi}{\xi} - 2\psi B - a - a\xi B, \end{aligned} \quad (2.5)$$

where (1.7) and (2.3) are given by

$$B(0) = 0, \quad \psi(0) = 0 \quad (2.6)$$

and

$$B \sim -\frac{1}{\xi}, \quad \psi \sim -\frac{1}{a\xi} \quad \text{as } \xi \rightarrow \infty. \quad (2.7)$$

Of course, this reduction from a four-dimensional system to a three-dimensional system is made possible by the fact that equation (1.6) is invariant under phase shifts.

We prove theorem 2.1 by analysing the solutions of equation (2.5) that satisfy the initial and asymptotic conditions (2.6) and (2.7), respectively, beginning with those that satisfy (2.7). These solutions form a three-dimensional manifold in the $A - B - \psi - \xi - d$ extended phase space, and we denote this manifold by M^{∞} , where the superscript ∞ corresponds to the fact that they satisfy (2.7). By tracking these solutions from ∞ back to $\xi = \xi_{\max} = (2 - \sqrt{a})/a$ (see figure 2), we find that, at ξ_{\max} , a segment of the manifold M^{∞} is nearly a horizontal line

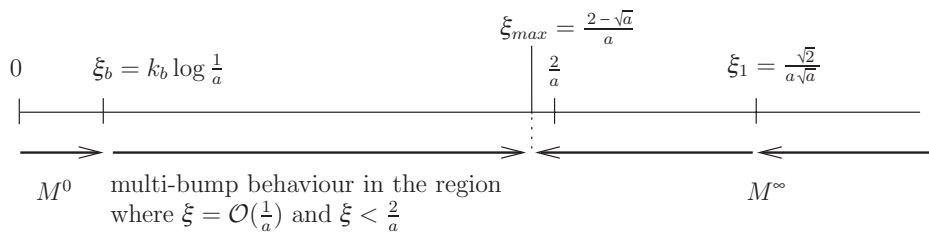


Figure 2. The different points and intervals on the ξ -axis. As explained in section 2, solutions on the manifolds M^∞ and M^0 are tracked to ξ_{\max} from ∞ and 0, respectively, and it is shown that these manifolds have two families of transverse intersection points at ξ_{\max} . The multi-bump, self-similar, blowup solutions of theorem 2.1 lie in these transverse intersections.

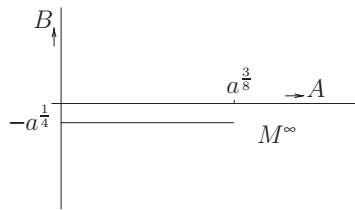


Figure 3. A sketch of the manifold M^∞ in the A - B plane at $\xi = \xi_{\max}$.

segment that stretches out at least over the interval $(0, a^{3/8}]$ in the A coordinate with $B = -a^{1/4}$ to leading order (see figure 3).

Next, we turn to the solutions of (2.5) that satisfy the initial condition (2.6). These solutions also form a three-dimensional manifold, which we denote by M^0 . We track the solutions on M^0 from $\xi = 0$ to $\xi = \xi_{\max}$ in two stages (see figure 2). First, in section 4, we track M^0 forwards to $\xi = \xi_b = k_b \log(1/a)$, for some $k_b > 0$.

Then, in sections 5–7, we track the solutions on M^0 further forwards through the interval (ξ_b, ξ_{\max}) inside which the bumps lie. We will introduce a ‘slow’, independent variable $\eta = a\xi$ and the shifted phase variable $\phi = \psi + (a\xi/2)$ in (2.5). Under the assumption that $|\phi| < a$ (which is verified for the desired range of ξ values in section 8), the governing system becomes

$$\begin{aligned} A_\xi &= AB, \\ B_\xi &= 1 - \frac{\eta^2}{4} - B^2 - A^2 + a \frac{(1-d)B}{\eta} + \text{hot}, \\ \eta_\xi &= a. \end{aligned} \tag{2.8}$$

The higher order terms in the equation for B contain the ϕ^2 term.

The global geometry of the invariant manifolds of (2.8) is studied in sections 5 and 6. For $a = 0$, the system (2.8) is a planar Hamiltonian system depending on a fixed parameter η , and it has a pair of saddle fixed points connected by a pair of heteroclinic orbits that enclose a family of periodic orbits for each $\eta \in (0, 2)$. Then, for $0 < a \ll 1$, geometric singular perturbation theory [11, 17] identifies the persistent manifolds, and adiabatic Melnikov function theory enables us to calculate the splitting distance between—and critical intersection points of—the relevant invariant manifolds.

This global geometric information is then used in section 7 to track solutions on M^0 further forwards to $\eta = \eta_{\max} = a\xi_{\max}$. We will show that, on the cross section $\eta = \eta_{\max}$ in the A - B plane, M^0 exhibits a highly complex structure (see figure 9). Most importantly, on the cross section $\eta = \eta_{\max}$ in the A - B plane, there are two families of transverse intersection points of

the manifolds M^0 and M^∞ . Hence, there exist two families of solutions on M^0 and M^∞ such that for each member of these families the A and B coordinates are the same at η_{\max} . (The values differ from member to member, of course.) The properties of these solutions are further specified in section 9. We note here that one of the main properties is that the A coordinates at ξ_{\max} of the intersection points lie exponentially close to zero for one family while they are at $\mathcal{O}(a^{3/8})$ for the other family.

The above analysis almost completes the proof of theorem 2.1. The last step involves the ψ coordinates. We observe that the ψ coordinates of the solutions just identified need not coincide, in general. Hence, in section 10, we show that the interval of values of the ψ coordinates of the relevant points on M^0 overlaps the interval of values of the ψ coordinates of the relevant points on M^∞ . Furthermore, we prove that the derivative of the ψ coordinate of points on M^0 is much larger than that same derivative for points on M^∞ . See figure 11 for a sketch of the manifolds in the d - ψ plane. Hence, we will be able to conclude that, for each member of the two families identified above and for each a sufficiently small, there exists a unique d such that not only the A and B coordinates of the solutions on both manifolds are the same but their ψ coordinates are the same, as well. In conclusion, the above analysis shows that the three-dimensional manifolds M^0 and M^∞ have two families of transverse intersection points in the $A - B - \psi - \xi - d$, extended, five-dimensional phase space and, hence, that the locally unique, multi-bump solutions claimed in theorem 2.1 exist.

Remark 2.2. The analysis required for the multi-bump solutions studied in this paper is much finer than that needed for the ground state (1-bump) studied in [23,35]. The estimates in [23,35] could be coarse over the midrange. For example, in [35] the manifold M^∞ is pulled back much further than to ξ_{\max} , there, it is integrated backwards all the way to $\xi_b = k_b \log(1/a)$ for some constant k_b , assuming that the solutions are monotone. Here, however, the interesting phenomenon, namely the extra bumps, occurs precisely in the midrange.

Remark 2.3. Several of the main ideas and techniques used in this paper can also be used to help show the existence of the multi-bump solutions with $K = 0$ and $J = 1, 2, \dots$

Remark 2.4. In the proofs throughout this paper, the letter c is used to denote various positive, $\mathcal{O}(1)$ constants. These constants are local.

3. The manifold M^∞ of solutions satisfying the asymptotic conditions at ∞

In this section, we study the manifold of solutions that satisfy the condition (2.3). We denote it by M^∞ , and we focus on the behaviour of the solutions on M^∞ as they are integrated backwards to where ξ equals $\xi_{\max} = (2 - \sqrt{a})/a$. This analysis is decomposed into two steps. First, we show that the solutions that lie on M^∞ are well understood for ξ very large, that is, for $\xi > (\sqrt{2}/a\sqrt{a})$. Then, we will integrate the solutions on M^∞ back further to determine the position of M^∞ at $\xi_{\max} = (2 - \sqrt{a})/a$.

3.1. Tracking M^∞ backwards to $\xi = (\sqrt{2}/a\sqrt{a})$

The behaviour of solutions on M^∞ for ξ very large was already studied in [23,35]. The results are stated in the following theorem.

Theorem 3.1. *Assume that $d > 2$ is fixed and that $d - 2$ and a are sufficiently small. Then, for every $\xi \geq (\sqrt{2}/a\sqrt{a})$ and A_1 sufficiently small, there is a unique solution to (2.5) that satisfies the boundary condition (2.7) and $A(\xi) = A_1$.*

The proof of this theorem is an application of the contraction mapping principle to a rescaled form of system (2.5). We will not give it here, instead we refer to theorem 3.1 in [35].

Theorem 3.1 gives us a solution satisfying the boundary condition (2.7) that is characterized by its amplitude at $\xi_1 = (\sqrt{2}/a\sqrt{a})$ and the value of d . This means that choosing $A(\xi_1)$ and d gives a locally unique solution that is a function of ξ . Thus, the manifold M^∞ of solutions that satisfy the boundary condition is of dimension 3 in (A, B, ψ, ξ, d) -space.

3.2. Tracking M^∞ backwards further to $\xi_{\max} = (2 - \sqrt{a})/a$

In this section, we study the behaviour of the solutions on M^∞ as they are integrated backwards further from $\xi_1 = (\sqrt{2}/a\sqrt{a})$ to $\xi_{\max} = (2 - \sqrt{a})/a$. We denote the values of A, B , and ψ at $\xi = \xi_{\max}$ by $A_d^\infty(\xi_{\max}), B_d^\infty(\xi_{\max})$, and $\psi_d^\infty(\xi_{\max})$. The goal is to show that $B_d^\infty(\xi_{\max})$ lies close to $-a^{1/4}$ in a C^1 manner (see lemmas 3.2 and 3.5) and that $\psi_d^\infty(\xi_{\max})$ lies close to $(-a\xi_{\max}/2)$ (see lemma 3.2). Also, for these solutions, we will show that the interval of values assumed by $A_d^\infty(\xi_{\max})$ stretches to include the interval $(0, a^{(3/8)})$. In figure 3, a sketch of the manifold M^∞ is given in the A - B plane.

We proceed largely in the same way as in [23, 35], by introducing a rescaling of Q for which the linearized equation (2.1) for Q becomes self-adjoint. Let $Q(\xi) = X(\xi)W(\xi)$, where X is chosen so that, after substitution in (1.6), the equation for W does not contain any first-order derivatives (i.e. the linearized equation for W is self-adjoint). This gives $X(\xi) = e^{-(ia/4)\xi^2} \xi^{(1-d)/2}$ and the following equation for W :

$$W_{\xi\xi} + \left(\frac{a^2\xi^2}{4} - 1 - \frac{ia}{2}(d-2) - \frac{1}{4\xi^2}(d-1)(d-3) \right) W + \xi^{1-d}|W|^2W = 0. \tag{3.1}$$

The linearized version of this equation is

$$W_{\xi\xi} + \left(\frac{a^2\xi^2}{4} - 1 - \frac{ia}{2}(d-2) - \frac{1}{4\xi^2}(d-1)(d-3) \right) W = 0, \tag{3.2}$$

which reduces for d near 2 and $\xi \gg 1$ to the parabolic cylinder equation

$$W_{\xi\xi} + \left(\frac{a^2\xi^2}{4} - 1 \right) W = 0. \tag{3.3}$$

At $\xi = 2/a$, the coefficient in front of the W term vanishes, and therefore the equation type of (3.2) changes at that point from elliptic for $\xi > 2/a$ to hyperbolic for $\xi < 2/a$.

In the elliptic regime, the two linearly independent solutions of (3.3) are given to leading order by

$$W_1 = \xi^{(d-3)/2-i/a} e^{(ia/4)\xi^2} \quad \text{and} \quad W_2 = \xi^{(1-d)/2+i/a} e^{(-ia/4)\xi^2}. \tag{3.4}$$

The higher order terms are small as long as $\xi \gg 2/a$ and $a \ll 1$. Since the value of (1.2) along W_2 does not vanish, it is not the solution we are looking for (see section 2). Instead, W_1 has the correct asymptotics at infinity.

To determine approximations for $B_d^\infty(\xi_{\max})$ and $\psi_d^\infty(\xi_{\max})$, we study solutions of (3.3) close to the turning point to obtain an estimate (see lemma 3.1) for the linearized equation (2.1). We denote these approximations by $B_{d,\text{lin}}^\infty(\xi_{\max})$ and $\psi_{d,\text{lin}}^\infty(\xi_{\max})$. Then, we show (see lemma 3.2) that the results remain essentially the same for the full nonlinear equation (1.6) for Q .

Lemma 3.1. *For $d > 2$ fixed and for $d - 2$ and a sufficiently small,*

$$B_{d,\text{lin}}^\infty(\xi_{\max}) = -a^{1/4} + \frac{1}{4}\sqrt{a} + \text{hot},$$

$$\psi_{d,\text{lin}}^\infty(\xi_{\max}) + \frac{a\xi_{\max}}{2} \text{ is exponentially small.}$$

This lemma, proved in appendix A, follows from the explicit expression for the leading order solution of (3.3) and the relations between A , B , ψ , and W ,

$$\begin{aligned} A &= |Q| = \xi^{(1-d)/2} |W|, \\ B &= \operatorname{Re} \left(\frac{W_\xi}{W} \right) + \frac{1-d}{2\xi}, \\ \psi &= \operatorname{Im} \left(\frac{W_\xi}{W} \right) - \frac{a\xi}{2} \end{aligned} \quad (3.5)$$

(see also [2] and chapter 8.1 of [36]).

Next, we show that essentially the same approximations hold for the solutions of the full equation (3.1) and, hence, also for (1.6).

Lemma 3.2. *For $d > 2$ fixed and for $d - 2$ and a sufficiently small, there exists a positive constant c_1 such that*

$$B_d^\infty(\xi_{\max}) = -a^{1/4} + c_1 \sqrt{a}$$

and

$$\psi_d^\infty(\xi_{\max}) + \frac{a\xi_{\max}}{2} \text{ is exponentially small.}$$

Proof. We introduce amplitude and phase coordinates associated to W :

$$W(\xi) = y(\xi) \exp \left[i \int_0^\xi \phi(x) dx \right], \quad z(\xi) = \frac{y_\xi}{y}. \quad (3.6)$$

These are analogous to the coordinates A , B , and ψ associated to Q . Moreover, (3.5) and (3.6) imply the following relations between B and z and between ψ and ϕ :

$$\begin{aligned} z &= \frac{d-1}{2\xi} + B, \\ \phi &= \frac{a\xi}{2} + \psi. \end{aligned} \quad (3.7)$$

Equation (3.1) may be written in the variables y , z , and ϕ as

$$\begin{aligned} y_\xi &= yz, \\ z_\xi &= \phi^2 - \frac{a^2 \xi^2}{4} + 1 - z^2 + \frac{1}{4\xi^2} (d-1)(d-3) - \xi^{1-d} y^2, \\ \phi_\xi &= -2\phi z + \frac{a}{2} (d-2). \end{aligned} \quad (3.8)$$

We will compare the solutions of (3.8) to the solutions of the linear equation (3.2) obtained in lemma 3.1. Let $\hat{z}(\xi) = z(\xi) - \bar{z}(\xi)$ and $\hat{\phi}(\xi) = \phi(\xi) - \bar{\phi}(\xi)$, where $\bar{z}(\xi)$ and $\bar{\phi}(\xi)$ are the solutions of the linearized system (3.2). Note that in the amplitude and phase coordinates linearization corresponds to setting $y = 0$, so that the linearized system depends only on z and ϕ . The estimates for B and ψ in lemma 3.1 imply that $\bar{z} = -a^{1/4} + \frac{1}{4}\sqrt{a}$ and $\bar{\phi}$ is exponentially small to leading order at $\xi = \xi_{\max}$. We will show here that $|\hat{z}| < \sqrt{a}$ and that $\hat{\phi}$ is exponentially small for $\xi \geq \xi_{\max}$. Combining these two results, we find approximations for z and ϕ . Finally, these approximations can be translated, via (3.7), into the desired approximations for B and ψ .

The system (3.8) can be written in terms of y , \hat{z} , and $\hat{\phi}$ as

$$\begin{aligned} y_\xi &= y\bar{z} + y\hat{z} \\ \begin{pmatrix} \hat{z}_\xi \\ \hat{\phi}_\xi \end{pmatrix} &= \begin{pmatrix} -2\bar{z} & 2\bar{\phi} \\ -2\bar{\phi} & -2\bar{z} \end{pmatrix} \begin{pmatrix} \hat{z} \\ \hat{\phi} \end{pmatrix} + \begin{pmatrix} \hat{\phi}^2 - \hat{z}^2 - \xi^{1-d} y^2 \\ -2\hat{\phi}\hat{z} \end{pmatrix}. \end{aligned} \quad (3.9)$$

The \hat{z} - and $\hat{\phi}$ -equations have been written in this way, following [23] and [35], to show the structure of the 2×2 matrix, whose behaviour plays an important role in the analysis. For $\xi \gg 2/a$ we have that $\bar{z} \sim -(3-d)/2\xi < 0$ (because $\bar{z} = \text{Re}[(d/d\xi)|W|/|W|]$ from the definition of the polar coordinates (3.6) and because we evaluate along W_1). We need to ascertain that $\bar{z} \leq 0$ for every $\xi \geq \xi_{\max}$. For $\xi \gg 1$ and $a \ll 1$, the solutions to (3.3) can be used to calculate the sign of \bar{z} . A solution to (3.3) can be written as

$$W = K W \left(\frac{1}{a}, \sqrt{a}\xi \right) + \frac{i}{2} e^{-(\pi/a)} W \left(\frac{1}{a}, -\sqrt{a}\xi \right), \tag{3.10}$$

where the functions on the right-hand side are Weber parabolic functions (see [1]), and K is a constant. Computation of $\bar{z} = \text{Re}[(d/d\xi)|W|/|W|]$ shows that $\bar{z} < 0$ at $\xi = 2/a$ (for $a \ll 1$), and \bar{z} decreases monotonically and algebraically to 0 as ξ increases, so that $\bar{z} < 0$ for $\xi \geq \xi_{\max}$.

Define $\xi_2 < \xi_1 = (\sqrt{2}/a\sqrt{a})$ by $\bar{z}(\xi_2) = -2a$. Such a ξ_2 exists because $\bar{z} \sim -a^{-(1/4)}$ at ξ_{\max} , \bar{z} increases monotonically for $\xi \geq \xi_{\max}$, and $\bar{z} \sim -((3-d)/2\sqrt{2})a^{3/2}$ at ξ_1 . It remains to show that, for $y(\xi_1)$ in some appropriate range, $|\hat{z}| < \sqrt{a}$ and that $\hat{\phi}$ is exponentially small for $\xi \geq \xi_{\max}$. The estimate for \hat{z} is conservative; \hat{z} is exponentially small for $\xi > \xi_2$.

To show this, we need the following lemma.

Lemma 3.3. *We denote by \mathcal{V} the space of solutions to (3.9) that satisfy*

- (a) $(y, \hat{z}, \hat{\phi})$ is exponentially small for $\xi_2 \leq \xi \leq \xi_1$;
- (b) $|y| < 2a^{-(1/8)}$, $|\hat{z}| < \sqrt{a}$, and $\hat{\phi}$ is exponentially small for $\xi \geq \xi_{\max}$.

Then, for $y(\xi_1)$ chosen appropriately, sufficiently small, the solutions remain in this space.

The proof of this lemma is given in appendix B, and it is based on an argument that uses continuous induction. We first show that if $y(\xi)$ is exponentially small for $\xi \geq \xi_2$, then \hat{z} and $\hat{\phi}$ are exponentially small for $\xi \geq \xi_2$, provided that they are already this small at $\xi = \xi_1$. Vice versa, we show that if \hat{z} is exponentially small for $\xi \geq \xi_2$ and y is exponentially small at ξ_1 , then for $y(\xi_1)$ chosen small y is also exponentially small for $\xi \geq \xi_2$. If we can prove the above two statements, then we know that the solution satisfies the first property of the space. The same type of argument can be used to show that the solutions also satisfy property (b).

Using this lemma, we can complete the proof of lemma 3.2. We choose $y(\xi_1)$ so that lemma 3.3 is satisfied. Then, it follows immediately that $\hat{\phi}$ is exponentially small and $|\hat{z}| < \sqrt{a}$ for every $\xi \geq \xi_{\max}$. □

In the following lemma, we estimate $A_d^\infty(\xi_{\max})$.

Lemma 3.4. *For $d > 2$ fixed and for $d - 2$ and a sufficiently small, the range of $A_1 = A(\sqrt{2}/a\sqrt{a})$ can be chosen such that, as a function of A_1 , $A_d^\infty(\xi_{\max})$ is onto $(0, a^{3/8}]$.*

Proof. We use the relation $A = \xi^{(1-d)/2}y$, between y and A that follows from the relation between Q and W . The proof of lemma 3.2 shows that one may choose the range of $y(\xi_1)$ such that $y < 2a^{-1/8}$ for all $\xi \geq \xi_{\max}$. In the proof of lemma 3.2, we chose $y(\xi_1)$ in an interval such that $y(\xi_2)$ is exponentially small. For the largest value of $y(\xi_1)$ we know that $y(\xi_{\max}) > \sqrt{2}a^{-1/8}$. Thus, $A_d^\infty(\xi_{\max}) > a^{3/8}$ since $\xi_{\max}^{(1-d)/2} > \sqrt{a/2}$. □

We conclude this section with a lemma extending the C^0 closeness of $B_d^\infty(\xi_{\max})$ to $-a^{1/4}$ in the A - B plane to C^1 closeness. This result will then be used in section 7 to establish the transversality of M^0 and M^∞ .

Lemma 3.5. *For $d > 2$ fixed, for $d - 2$ and a sufficiently small, and for each A_1 in the range of A_1 values found in lemma 3.4, the map*

$$A_1 \rightarrow (A_d^\infty(\xi_{\max}, A_1), B_d^\infty(\xi_{\max}, A_1))$$

has a slope that is less than $ca^{1/8}$ in the A - B plane for some $c > 0$.

Proof. Define $Z = \partial z / \partial A_1$, $Y = \partial y / \partial A_1$, and $\Psi = \partial \phi / \partial A_1$. Then Z , Y , and Ψ satisfy the variational equations,

$$\begin{aligned} Y_\xi &= (\bar{z} + \hat{z})Y + yZ, \\ \begin{pmatrix} Z_\xi \\ \Psi_\xi \end{pmatrix} &= \begin{pmatrix} -2\bar{z} & 2\bar{\phi} \\ -2\bar{\phi} & -2\bar{z} \end{pmatrix} \begin{pmatrix} Z \\ \Psi \end{pmatrix} + \begin{pmatrix} 2\hat{\phi}\Psi - 2\hat{z}Z - 2\xi^{1-d}Yy \\ -2\hat{\phi}Z - 2\hat{z}\Psi \end{pmatrix}. \end{aligned} \quad (3.11)$$

Since Y stays bounded away from 0, we may look at the quantities Z/Y and Ψ/Y . These satisfy the equations

$$\begin{pmatrix} \left(\frac{Z}{Y}\right)_\xi \\ \left(\frac{\Psi}{Y}\right)_\xi \end{pmatrix} = \begin{pmatrix} -3\bar{z} - 3\hat{z} & 2\bar{\phi} + 2\hat{\phi} \\ -2\bar{\phi} - 2\hat{\phi} & -3\bar{z} - 3\hat{z} \end{pmatrix} \begin{pmatrix} \frac{Z}{Y} \\ \frac{\Psi}{Y} \end{pmatrix} - \begin{pmatrix} y \left(\frac{Z}{Y}\right)^2 + 2\xi^{1-d}y \\ y \left(\frac{Z}{Y}\right) \left(\frac{\Psi}{Y}\right) \end{pmatrix}. \quad (3.12)$$

Integrating backwards to ξ_{\max} and using an appropriate integrating factor similar to that in the proof of lemma 3.3, we have that Z/Y and Ψ/Y can be estimated by $2a^{-1/4}\xi^{1-d}y$ (since \bar{z} dominates \hat{z} , and $\bar{z} \approx -a^{-1/4}$ and negative for $\xi \geq \xi_{\max}$). Also, we know that $y < 2a^{-1/8}$. Therefore, $(\partial z / \partial A_1) / (\partial y / \partial A_1) = Z/Y \leq \xi^{1-d}y$, and so $(\partial B / \partial A_1) / (\partial A / \partial A_1) \leq 2a^{-1/4}\xi^{(1-d)/2}y \ll ca^{1/8}$, for some positive constant c . \square

Remark 3.1. More generally, we can pull back M^∞ to a point $\xi = (2-b)/a$, where $a^{2/3} \ll b \ll a^{2/5}$. The choice of $b = \sqrt{a}$, used to obtain ξ_{\max} , was made to simplify the analysis. Further details are given in remark 7.2, after the necessary analysis of M_0 is presented.

4. Tracking the manifold M^0 forwards to $\xi_b = k_b \log(1/a)$

In this section, we track solutions on M^0 forwards to a point $\xi = \xi_b = k_b \log(1/a)$ where k_b satisfies a condition given in the lemmas below. The main results are stated in lemmas 4.1 and 4.2. We denote the values of A , B , and ψ at $\xi = \xi_b$ by $A_d^0(\xi_b)$, $B_d^0(\xi_b)$, and $\psi_d^0(\xi_b)$. Some of the necessary analysis was already carried out in [23, 35].

Lemma 4.1. *There exist $B^- < -1 < B^+ < 0$, a positive τ less than ξ_b , and an interval I such that trajectories with $A(0) \in I$, $B(0) = 0$, $\phi(0) = 0$ satisfy $B^- < B(\xi) < B^+$ for all $\tau \leq \xi \leq \xi_b$ and, at $\xi = \xi_b$, the B coordinate lies in an interval with endpoints B^- and B^+ .*

Lemma 4.2. *For the trajectories satisfying $B^- < B(\xi) < B^+$ for $\tau \leq \xi \leq \xi_b$, $A(0) \in I$, $B(0) = 0$, $\phi(0) = 0$, we have that $c_1 a^{1/2} < A_d^0(\xi_b) < c_2 a^{l_1}$, where $l_1 < \frac{1}{2}|B^+|k_1$, $k_1 = \min\{(\ell - 1 - d)/2|B^-|, 1/2|B^-|\}$ and c_1, c_2 are positive constants. In addition, $\xi = \xi_b = k_b \log(1/a)$, with $\frac{1}{2}k_1 < k_b < k_1$.*

Lemma 4.1 is lemma 5.5 in [35] and lemma 4.2 is an improved version of lemma 5.6 in [35]. These results are illustrated in figure 4. We refer to [35] for the proof of lemma 4.1 and we will now prove lemma 4.2 here. Also, note that the τ found here is different from the one defined in (1.5).

Proof. From the first equation of system (2.5) one has $A(\xi_b) = A(\tau) \exp(\int_\tau^{\xi_b} B(s) ds)$. Now, because $B^- < B(\xi) < B^+$, one has

$$A(\tau)e^{B^-(\xi_b-\tau)} < A(\xi_b) < A(\tau)e^{B^+(\xi_b-\tau)}.$$

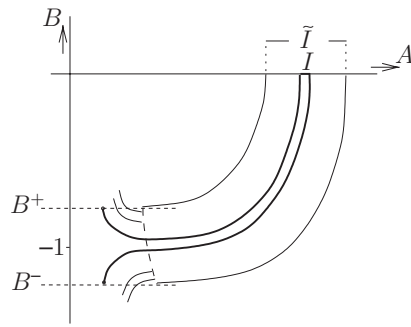


Figure 4. There exists an exponentially small subinterval I of \tilde{I} such that trajectories of (2.5) with initial conditions in I stay between B^- and B^+ for all $\tau \leq \xi \leq \xi_b$. The dashed curve is the image of \tilde{I} at $\xi = \tau$. Trajectories from that curve may stay between B^- and B^+ for $\xi \leq \xi_b$ or they may leave that region, but they may not enter it.

Setting $c_1 = A(\tau)e^{|B^-|\tau}$ and $c_2 = A(\tau)e^{|B^+|\tau}$ we find that the above inequality becomes $c_1 e^{B^- \xi_b} < A(\xi_b) < c_2 e^{B^+ \xi_b}$. In turn, using the definition $\xi_b = k_b \log(1/a)$, we obtain

$$c_1 a^{|B^-|k_b} < A(\xi_b) < c_2 a^{|B^+|k_b}.$$

Next, we assume that $0 < k_b < 1/2|B^-|$, which implies that $A(\xi_b) \gg c_1 a^{1/2}$. We combine this condition on k_b together with the requirement, $0 < k_b < (\ell - 1 - d)/2|B^-|$, that we will need to impose below in lemma 8.2. This leads to $0 < k_b < k_1$, where we define $k_1 = \min\{(\ell - 1 - d)/2|B^-|, 1/2|B^-|\}$. Finally, choosing $\frac{1}{2}k_1 < k_b < k_1$ we find that $A(\xi_b) \ll c_2 a^{l_1}$, where $l_1 < \frac{1}{2}k_1|B^+|$ which gives the statement of the lemma. Note that the choice of $\frac{1}{2}$ both for the power of a in the lower bound on $A(\xi_b)$ and for the factor in front of k_1 in the lower bound on k_b are made for simplicity of the analysis; more generally, both factors can be replaced by any real number in $(0, 1)$. \square

The solutions on M^0 are studied by comparing them to the ground state solution, of equation (1.4):

$$R_{\xi\xi} + \frac{R_\xi}{\xi} - R + R^3 = 0.$$

Recall that R_1 is positive and vanishes as $\xi \rightarrow \infty$ (see [7, 29]). Most solutions of system (2.5) that satisfy the initial conditions (2.6) do not stay close to the ground state solution, including the solution for which $A(0) = R_1(0)$. However, there exists an interval of parameter values for $A(0)$ for which the solution of (2.5) does stay close to $R_1(\xi)$ for $\xi \leq \xi_b$.

First, an interval \tilde{I} and constants B^- and B^+ , where $B^- < -1 < B^+ < 0$, are found such that the solutions satisfying $A(0) \in \tilde{I}$, $B(0) = 0$, and $\psi(0) = 0$ at $\xi = \tau$ form a curve whose endpoints lie on B^- and B^+ (see figure 4). For these solutions $A_d^0(\xi_b)$ is strictly smaller than a^3 . Next, it is shown that on $B = B^+$ one has $B_\xi > 0$, and that on $B = B^-$ one has $B_\xi < 0$, for all $\tau < \xi \leq \xi_b$. Finally, a subinterval $I \subset \tilde{I}$ can be found such that solutions with $A(0) \in I$, $B(0) = 0$, and $\psi(0) = 0$ stay in the interval $[B^-, B^+]$ for all $\tau \leq \xi \leq \xi_b$ and such that at $\xi = \xi_b$ the endpoints are B^- and B^+ . Moreover, the image at ξ_b of points on I transversely intersects the line $B = -1$ in the A - B plane (see figure 4).

5. Global theory for the invariant manifolds of system (2.8)

Let $\eta_{\min} = a\xi_b$ and $\eta_{\max} = a\xi_{\max}$. We study the system (2.8) for $\eta > \eta_{\min}$, and we establish an asymptotic approximation for the position of M_0 on the slice η_{\max} . We start by studying

the geometry of system (2.8) for $a = 0$ and then apply the Fenichel theory to obtain the relevant information about the geometry for $0 < a \ll 1$. Then, by introducing an adiabatic Melnikov function, we obtain a more detailed view of the structure of the invariant manifolds of system (2.8) for $0 < a \ll 1$.

5.1. Geometry of the system (2.8) with $a = 0$

When $a = 0$, there exist three curves of fixed points,

$$\Gamma_{\pm}^0 = \left\{ (A, B, \eta) \mid A = 0, B = \pm \sqrt{1 - \frac{\eta^2}{4}}, \eta_{\min} < \eta < \eta_{\max} \right\} \quad (5.1)$$

and

$$\Gamma_0 = \left\{ (A, B, \eta) \mid A = \sqrt{1 - \frac{\eta^2}{4}}, B = 0, \eta_{\min} < \eta < \eta_{\max} \right\} \quad (5.2)$$

(see figure 5(a)). The curves Γ_{\pm}^0 are normally hyperbolic manifolds, since they are the unions of saddle fixed points $(A, B) = (0, \pm \sqrt{1 - (\eta^2/4)})$ for every fixed η (see figure 5(a)). Furthermore, for every $\eta \in (\eta_{\min}, \eta_{\max})$, these saddles are connected by a heteroclinic orbit. Finally, for every fixed η , there exists a one-parameter family of periodic orbits in the domain inside the heteroclinic orbit. This family limits on the centre fixed point $(A, B) = (A_{\text{ctr}}, 0) = (\sqrt{1 - (\eta^2/4)}, 0)$ (see figure 5(b)), and the curve Γ_0 shown in figure 5(a) is the union of these centres.

The leading part of system (2.8) can be written as the Duffing equation

$$A_{\xi\xi} = A \left(1 - \frac{\eta^2}{4} - A^2 \right). \quad (5.3)$$

Therefore, explicit expressions can be given for the heteroclinic and periodic orbits (see, e.g. [14]). Note that the variable B used here is the logarithmic derivative of A (see (2.4)). The heteroclinic orbit is given by

$$(A_0(\xi), B_0(\xi)) = [\sqrt{2}\alpha \operatorname{sech}(\alpha\xi), -\alpha \tanh(\alpha\xi)] \quad (5.4)$$

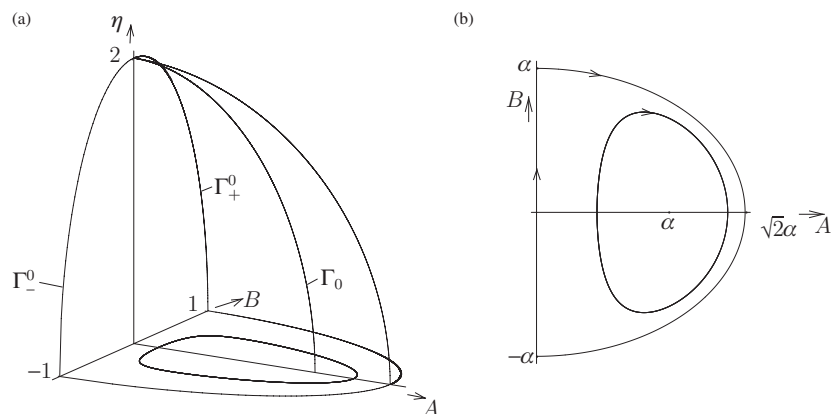


Figure 5. (a) A sketch of the three curves of critical points Γ_{\pm}^0 and Γ_0 in the A - B - η plane for $a = 0$. Here, the positive B -axis points into the paper. (b) The flow in the A - B plane for $\eta \in (\eta_{\min}, \eta_{\max})$ fixed, where $\alpha = \sqrt{1 - (\eta^2/4)}$.

for every $\eta_{\min} < \eta < \eta_{\max}$, where $\alpha = \sqrt{1 - (\eta^2/4)}$. We denote the manifold that consists of all these heteroclinic connections with $\eta_{\min} < \eta < \eta_{\max}$ by \mathcal{W} . The periodic solutions are given by

$$A^{(k)}(\xi) = \sqrt{2}\beta \operatorname{dn}(\beta\xi, k), \tag{5.5}$$

$$B^{(k)}(\xi) = -k^2\beta \frac{\operatorname{sn}(\beta\xi, k)\operatorname{cn}(\beta\xi, k)}{\operatorname{dn}(\beta\xi, k)}, \tag{5.6}$$

where $\beta = (\alpha/\sqrt{2-k^2})$ and $0 < k < 1$. Here, $k = 0$ corresponds to the centre point $(A, B) = (\sqrt{1 - \eta^2/4}, 0)$ and $k = 1$ to the heteroclinic solution. The period of such a solution is given by $T_0^{(k)} = 2(K(k)/\beta)$, where $K(k)$ is the complete elliptic integral of the first kind.

5.2. Persistence of the invariant manifolds for $0 < a \ll 1$ and their transverse intersections

Since the two curves of critical points Γ_{\pm}^0 are normally hyperbolic, we can apply the Fenichel theory [11, 17]. For $0 < a \ll 1$, Γ_{\pm}^0 persist, as long as η is restricted to $(\eta_{\min}, \eta_{\max})$ as slow manifolds Γ_+ and Γ_- , which lie $\mathcal{O}(a)$ close to Γ_+^0 and Γ_-^0 , respectively. These manifolds must also lie in the plane $\{A = 0\}$, since this remains an invariant plane for $a \neq 0$. Furthermore, it follows from the Fenichel theory that the manifolds Γ_+ and Γ_- have stable and unstable manifolds $\mathcal{O}(a)$ close to those of the unperturbed system. Let $W^u(\Gamma_+)$ denote the component of the unstable manifold of Γ_+ that lies $\mathcal{O}(a)$ close to the manifold \mathcal{W} for $\xi < 0$, and let $W^s(\Gamma_-)$ denote the component of the stable manifold of Γ_- that lies $\mathcal{O}(a)$ close to the manifold \mathcal{W} for $\xi > 0$. For $a > 0$ these manifolds no longer coincide, as they did for $a = 0$.

Now, we will study the behaviour of the unstable manifold of Γ_+ , $W^u(\Gamma_+)$, and the stable manifold of Γ_- , $W^s(\Gamma_-)$, for $0 < a \ll 1$. The Melnikov method for slowly varying systems (see [30, 34]), yields an expression for the distance between $W^u(\Gamma_+)$ and $W^s(\Gamma_-)$ as a function of η . In fact, denoting the first intersection of $W^u(\Gamma_+)$ with the set $\{B = 0, A > 0\}$ by $P(\Gamma_+)$, and similarly the first intersection of $W^s(\Gamma_-)$ with the same set by $P^{-1}(\Gamma_-)$, we find the distance between $P(\Gamma_+)$ and $P^{-1}(\Gamma_-)$.

Remark 5.1. The Fenichel and Melnikov theorems may be used directly to obtain the desired results for all $\eta \in (0, 2)$. Here, we are also interested in the behaviour of $W^u(\Gamma_+)$ and $W^s(\Gamma_-)$ up to $\eta_{\max} = 2 - \sqrt{a}$ and we note that after a suitable rescaling (the eigenvalues are of size $\mathcal{O}(\sqrt{a})$ but the perturbation is of size $\mathcal{O}(a)$) the Fenichel and Melnikov theories can also be applied up to η_{\max} .

To apply the Melnikov method, we transform system (2.8) by introducing $C = AB$ so that it is explicitly divergence-free,

$$\begin{aligned} A_{\xi} &= C, \\ C_{\xi} &= A \left(1 - \frac{\eta^2}{4} - A^2 \right) + a \frac{(1-d)C}{\eta} + \text{hot}, \\ \eta_{\xi} &= a. \end{aligned} \tag{5.7}$$

In this representation, the plane $B = 0$ corresponds to the plane $C = 0$, and to leading order, system (5.7) is the Duffing equation.

For any η_0 such that $\eta_{\min} < \eta_0 < \eta_{\max}$, we define A_a^u and A_a^s as the η_0 -dependent intersection points of orbits on $W^u(\Gamma_+)$ and $W^s(\Gamma_-)$, respectively, with $\{\eta = \eta_0\}$ on $C = 0$. The solutions $\gamma_a^u(\xi) = (A_a^u(\xi), C_a^u(\xi), \eta_a^u(\xi))$ in $W^u(\Gamma_+)$ and $\gamma_a^s(\xi) = (A_a^s(\xi), C_a^s(\xi), \eta_a^s(\xi))$ in $W^s(\Gamma_-)$ for the perturbed system (5.7) are determined by the initial

condition $\gamma_a^{u,s}(\xi) = (A_a^{u,s}(\xi), 0, \eta_0)$. Also, $\gamma_0(\xi) = (A_0(\xi), C_0(\xi), \eta_0)$ is the homoclinic solution of the unperturbed system with $\gamma_0(0) = (\sqrt{2(1 - (\eta_0^2/4))}, 0, \eta_0)$. Here, A_0 and C_0 are given explicitly by (5.4), where $C_0 = A_0 B_0$. We define the following ξ -dependent distance function:

$$\Delta(\xi, \eta_0) = \left\{ \left(\frac{\partial}{\partial a} (A_a^u(\xi) - A_a^s(\xi)) \right) \wedge \left(\begin{array}{c} C_0(\xi) \\ A_0(\xi) \left(1 - \frac{\eta_0^2}{4} - A_0(\xi)^2 \right) \end{array} \right) \right\}. \quad (5.8)$$

Then, from this ξ -dependent distance function, we derive the adiabatic Melnikov function in the usual way for slowly varying (or adiabatic) systems (see [30, 34]),

$$\Delta(0, \eta) = \int_{-\infty}^{\infty} \left\{ \left(\frac{0}{(1-d)C_0} \right) + \left(-\frac{0}{2} A_0 \right) \frac{\partial \eta}{\partial a} \right\} \wedge \left(\begin{array}{c} C_0 \\ A_0 \left(1 - \frac{\eta^2}{4} - A_0^2 \right) \end{array} \right) d\xi, \quad (5.9)$$

where $(\partial/\partial\xi)(\partial\eta/\partial a) = 1$ and $(\partial\eta/\partial a) = 0$ for $\xi = 0$ and hence $(\partial\eta/\partial a) = \xi$. Computing the integrals and using (5.4) and $C_0 = A_0 B_0$, we find

$$\begin{aligned} \Delta(0, \eta) &= \int_{-\infty}^{\infty} - \left[\frac{(1-d)C_0^2}{\eta} - \frac{\eta}{2} A_0 C_0 \xi \right] d\xi \\ &= -2\sqrt{1 - \frac{\eta^2}{4}} \left[\frac{2(1-d)}{3\eta} \left(1 - \frac{\eta^2}{4} \right) + \frac{\eta}{2} \right]. \end{aligned} \quad (5.10)$$

The function $\Delta(0, \eta)$ measures the distance between $P(\Gamma_+)$ and $P^{-1}(\Gamma_-)$ to $\mathcal{O}(a)$. Thus, by the Implicit Function theorem, a simple zero η_i of $\Delta(0, \eta)$ defines a transversal intersection point of $P(\Gamma_+)$ and $P^{-1}(\Gamma_-)$ at $B = 0$. We find that $\Delta(0, \eta) = 0$ for $\eta = \sqrt{4(d-1)/(d+2)}$ and for $\eta = 2$. However, since Δ is not defined at $\eta = 2$, only the first value of η is a sought-after zero of the adiabatic Melnikov function. Hence, the two manifolds intersect transversely in a point that is $\mathcal{O}(a)$ close to $(\sqrt{2(1 - (\eta_i^2/4))}, 0, \eta_i)$ with $\eta_i = \sqrt{4(d-1)/(d+2)}$. We label the η value of the actual intersection point by $\eta = \eta_{\text{zero}}$ (see figure 6(c)). Finally, η_i (and hence also η_{zero}) is one to leading order, since d is close to 2.

The adiabatic Melnikov function also gives the orientation of $W^u(\Gamma_+)$ with respect to $W^s(\Gamma_-)$ at $B = 0$. We find that $\Delta(0, \eta) > 0$ for $\eta_{\text{min}} < \eta < \eta_{\text{zero}}$; and, thus, $W^u(\Gamma_+)$ lies ‘outside’ $W^s(\Gamma_-)$, i.e. $p_1 > p_2$ for points $(p_1, 0, \eta) \in P(\Gamma_+)$ and $(p_2, 0, \eta) \in P^{-1}(\Gamma_-)$ (see figures 6(a) and (b)). Similarly, $\Delta(0, \eta) < 0$ for $\eta_{\text{zero}} < \eta < \eta_{\text{max}}$; and, therefore, $W^u(\Gamma_+)$ lies ‘inside’ $W^s(\Gamma_-)$, i.e. $p_1 < p_2$ for points $(p_1, 0, \eta) \in P(\Gamma_+)$ and $(p_2, 0, \eta) \in P^{-1}(\Gamma_-)$ (see figures 6(d) and (e)).

6. The images of $P(\Gamma_+)$ and $P^{-1}(\Gamma_-)$ and the locations of $W^u(\Gamma_+)$ and $W^s(\Gamma_-)$ on constant η slices

In this section, we study the images of $P(\Gamma_+)$ and the pre-images of $P^{-1}(\Gamma_-)$ on the set $\{B = 0, A > 0\}$, and then we use this information to determine the locations of long segments of the manifolds $W^u(\Gamma_+)$ and $W^s(\Gamma_-)$ on $\eta = \text{constant}$ slices. Recall that $P(\Gamma_+)$ and $P^{-1}(\Gamma_-)$ are the first intersections of $W^u(\Gamma_+)$ and $W^s(\Gamma_-)$, respectively, with the set $\{B = 0, A > 0\}$ (see figure 7).

The approach in this section is based in part on the work in [9, 10, 21, 22] as well as papers on the exchange lemma [17–20].

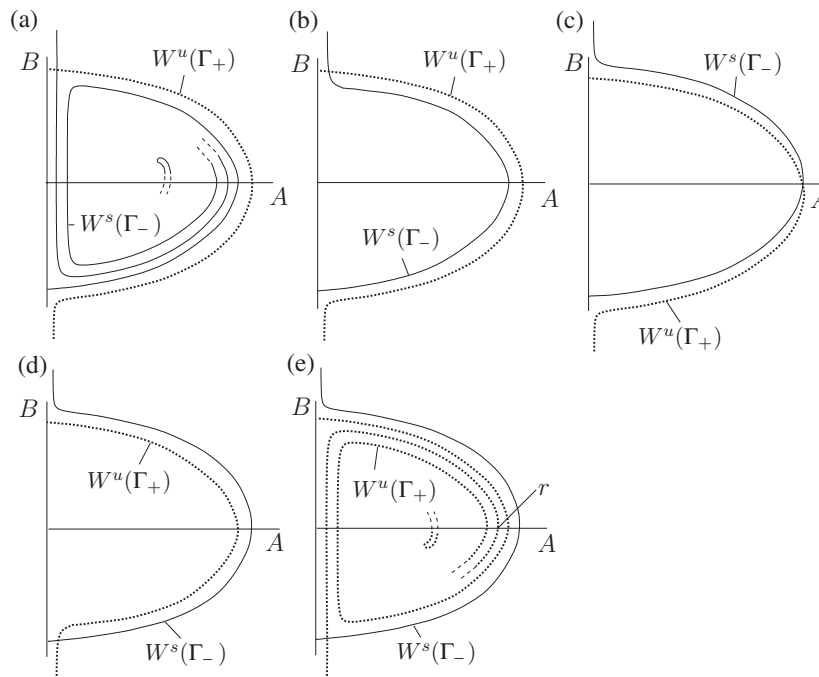


Figure 6. A sequence of sketches of the manifolds $W^u(\Gamma_+)$ ($\cdots\cdots$) and $W^s(\Gamma_-)$ (—) in the $A - B$ plane as η increases from η_{\min} to η_{\max} . Their positions are determined in sections 5 and 6. (a) At $\eta = \eta_{\min}$, $W^s(\Gamma_-)$ is curled up inside $W^u(\Gamma_+)$ and starts to pull back as η increases. As long as $\eta_{\min} \leq \eta < \eta_{\text{zero}}$, $W^u(\Gamma_+)$ lies ‘outside’ $W^s(\Gamma_-)$ at $B = 0$. The smaller the value of a , the more the tongue winds around the centre point, and hence in the sketch we only show the tip of the tongue and not all the spirals (b). (c) For $\eta = \eta_{\text{zero}}$, the two manifolds intersect at $B = 0$. Increasing η further (d), $W^u(\Gamma_+)$ starts to curl up inside $W^s(\Gamma_-)$ up to η_{\max} (e), where for $\eta_{\text{zero}} \leq \eta < \eta_{\max}$, $W^u(\Gamma_+)$ lies ‘inside’ $W^s(\Gamma_-)$ at $B = 0$.

6.1. The Poincaré map

To begin with, we need the Poincaré map of system (2.8). For $a = 0$, there exist two integrals of system (2.8):

$$\kappa_1 = \frac{1}{2}A^2B^2 - \frac{1}{2}\left(1 - \frac{\eta^2}{4}\right)A^2 + \frac{1}{4}A^4, \tag{6.1}$$

$$\kappa_2 = \eta. \tag{6.2}$$

Now, the Poincaré map is defined to be the map $\mathcal{P} : \Omega \rightarrow \Omega$ given by

$$\mathcal{P}(\kappa_1, \kappa_2) = (\kappa_1 + \Delta K_1(\kappa_1, \kappa_2), \kappa_2 + \Delta K_2(\kappa_1, \kappa_2)), \tag{6.3}$$

where Ω is the cross section

$$\Omega = \left\{ (A, B, \eta) \mid B = 0, \eta_{\min} < \eta < \eta_{\max}, \sqrt{1 - \frac{\eta^2}{4}} < A < \sqrt{2\left(1 - \frac{\eta^2}{4}\right) + c_3a} \right\} \tag{6.4}$$

for some $c_3 = \mathcal{O}(1)$, sufficiently large. The quantities $\Delta K_1(\kappa_1, \kappa_2)$ and $\Delta K_2(\kappa_1, \kappa_2)$ measure the accumulated change in the slow variables κ_1 and κ_2 of a solution of the perturbed system with initial data on the cross section Ω at its first return to Ω :

$$\Delta K_1(\kappa_1, \kappa_2) = \int_0^{T_a} \dot{\kappa}_1(A_a, B_a, \eta_a) d\xi \tag{6.5}$$

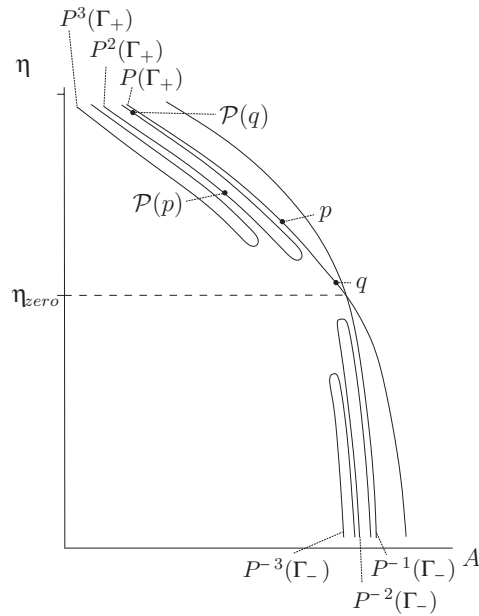


Figure 7. A sketch of the curves $P(\Gamma_+)$ and $P^{-1}(\Gamma_-)$ in the A - η plane (with $B = 0$) and of their intersection at $\eta = \eta_{\text{zero}}$. Also, the images of $P(\Gamma_+)$ and the pre-images of $P^{-1}(\Gamma_-)$ under the Poincaré map \mathcal{P} , $P^2(\Gamma_+)$, $P^3(\Gamma_+)$, ... and $P^{-2}(\Gamma_-)$, $P^{-3}(\Gamma_-)$, ... are sketched showing their tongue structure.

and

$$\Delta K_2(\kappa_1, \kappa_2) = \int_0^{T_a} \dot{\kappa}_2(A_a, B_a, \eta_a) d\xi. \tag{6.6}$$

Here, solutions of the perturbed system are denoted by (A_a, B_a, η_a) with return-time T_a .

Remark 6.1. The Poincaré map \mathcal{P} is well defined for points on $P(\Gamma_+)$ with $A < \sqrt{2(1 - (\eta^2/4))} + c_3a$, i.e. for that segment of $P(\Gamma_+)$ that lies inside $W^s(\Gamma_-)$, with $\eta_{\text{zero}} < \eta < \eta_{\text{max}}$, since the flow starting on Ω remains $\mathcal{O}(a)$ close to periodic orbits of the unperturbed system. Thus, the segment outside $W^s(\Gamma_-)$, i.e. with $\eta_{\text{min}} < \eta < \eta_{\text{zero}}$, has no image under \mathcal{P} (recall that η_{zero} is the value of η at which the actual intersection point of $P(\Gamma_+)$ and $P^{-1}(\Gamma_-)$ lies on $B = 0$). Similarly, \mathcal{P}^{-1} is only defined for that segment of $P^{-1}(\Gamma_-)$ that lies inside $W^u(\Gamma_+)$, i.e. for $\eta_{\text{min}} < \eta < \eta_{\text{zero}}$.

A solution (A_a, B_a, η_a) and its return-time T_a can be approximated by the solution $(A_{\text{un}}, B_{\text{un}}, \eta_{\text{un}})$ of the unperturbed system with period T_{un} that starts on the cross section Ω with the same initial data as (A_a, B_a, η_a) . Substituting the expressions for the integrals κ_1 and κ_2 , we obtain

$$\Delta K_1(\kappa_1, \kappa_2) = a \int_0^{T_{\text{un}}} \left(\frac{1-d}{\eta_{\text{un}}} A_{\text{un}}^2 B_{\text{un}}^2 + \frac{\eta_{\text{un}}}{4} A_{\text{un}}^2 \right) d\xi + \mathcal{O}(a^2) \tag{6.7}$$

and

$$\Delta K_2(\kappa_1, \kappa_2) = \int_0^{T_{\text{un}}} [a + \mathcal{O}(a^2)] d\xi = aT_{\text{un}} + \mathcal{O}(a^2). \tag{6.8}$$

The A_{un} and B_{un} are given by expressions (5.5) and (5.6) for $A^{(k)}$ and $B^{(k)}$, where the k is determined by the initial value of the solution. Note that for $\xi = 0$, the solution $(A^{(k)}, B^{(k)})$

intersects the cross section Ω , and for $\xi = T_{\text{un}}$ the solution has its first intersection point with Ω . Also, from (6.8) it immediately follows that $\Delta K_2 > 0$ for all κ_1 and κ_2 .

6.2. *The images of $P(\Gamma_+)$ and $P^{-1}(\Gamma_-)$ on Ω*

We will repeatedly apply the Poincaré map \mathcal{P} to $P(\Gamma_+)$ and its inverse \mathcal{P}^{-1} to $P^{-1}(\Gamma_-)$. Therefore, for each $n > 1$, we define

$$\begin{aligned} P^n(\Gamma_+) &\equiv \mathcal{P}^{n-1}(P(\Gamma_+)), \\ P^{-n}(\Gamma_-) &\equiv \mathcal{P}^{-n+1}(P^{-1}(\Gamma_-)) \end{aligned}$$

and we recall the conditions under which \mathcal{P} is well defined (see remark 6.1).

We construct the image $P^2(\Gamma_+)$ by focusing on the images of separate segments of $P(\Gamma_+)$, first on points whose η coordinates are exponentially close to η_{zero} and then on points whose η coordinates are not exponentially close to η_{zero} . A point q on $P(\Gamma_+) \cap \{\eta > \eta_{\text{zero}}\}$ whose η coordinate is exponentially close to, but not equal to, η_{zero} also lies exponentially close to $W^s(\Gamma_-)$. Therefore, if $\eta - \eta_{\text{zero}} = \mathcal{O}(e^{-c/a})$ for some $c > 0$ that is sufficiently large, then the orbit through q will first remain exponentially close to $W^s(\Gamma_-)$, enter a neighbourhood of Γ_- , then move towards Γ_+ , enter a neighbourhood of Γ_+ , and finally follow $W^u(\Gamma_+)$, again exponentially close to it, until it reaches $B = 0$ still exponentially close to $P(\Gamma_+)$. The η coordinate of $\mathcal{P}(q)$ is greater than that of q (see figure 7). Moreover, the closer a point q_1 lies on $P(\Gamma_+)$ to $\eta = \eta_{\text{zero}}$ the larger the η coordinate of $\mathcal{P}(q_1)$ is. Hence, there exists a point q_2 that is mapped by \mathcal{P} to a point exponentially close to $P(\Gamma_+)$ with $\eta = \eta_{\text{max}}$. This implies that only a segment of $P(\Gamma_+) \cap \{\eta > \eta_{\text{zero}}\}$ is mapped onto Ω . In addition, the points on this segment that lie exponentially close to η_{zero} are mapped by \mathcal{P} to a curve in that $A-\eta$ plane that lies exponentially close to $P(\Gamma_+)$ and stretches downwards from $\eta = \eta_{\text{max}}$ to some minimum value $\eta = \eta_2$.

On the other hand, for a point p on $P(\Gamma_+) \cap \{\eta > \eta_{\text{zero}}\}$ that does not lie exponentially close to η_{zero} , we can use the flow of the system to study the image under \mathcal{P} . We find that $\mathcal{P}(p)$ lies to the left and above the point p (see figure 7). More precisely, the change in both directions is of $\mathcal{O}(a)$; $|\mathcal{P}(p) - \bar{p}| = ca$ for some c , where \bar{p} is the point on $P(\Gamma_+)$ that has the same η coordinate as $\mathcal{P}(p)$. Thus, the points on the segment of $P(\Gamma_+)$ that do not lie exponentially close to η_{zero} are mapped to a curve that lies $\mathcal{O}(a)$ from $P(\Gamma_+)$ and stretches upwards to $\eta = \eta_{\text{max}}$.

Also, it is not possible for more than two points on $P(\Gamma_+) \cap \{\eta > \eta_{\text{zero}}\}$, with η sufficiently close to η_{zero} , to be mapped to points on $P^2(\Gamma_+)$ that have the same η value. This follows from the facts that the splitting distance between $W^u(\Gamma_+)$ and $W^s(\Gamma_-)$ grows monotonically as η is increased from η_{zero} (up to the value $\eta = \eta_{***}$, where η_{***} is the local maximum of $\Delta(0, \eta)$ that is well above η_2 but below η_{max}), and that the return-time for points on $P(\Gamma_+)$ under the map \mathcal{P} decreases monotonically when η is increased from η_{zero} .

Therefore, putting the pieces of information obtained above together and taking into account the fact that \mathcal{P} maps $P(\Gamma_+)$ continuously to Ω , we find that there is a segment of $P^2(\Gamma_+)$ that is a connected curve and that has the tongue structure of the type shown in figure 7. Here, by tongue structure, we mean that this segment of $P^2(\Gamma_+)$ doubly covers the interval $(\eta_2, \eta_{\text{max}})$ and that the two branches of this double covering are smoothly connected at the ‘tip’ of the tongue, which is the minimum at η_2 .

Applying the inverse of the Poincaré map on $P^{-1}(\Gamma_-)$ and using the same type of reasoning as above, we find that $P^{-2}(\Gamma_-)$ also has a tongue structure. More generally, the images $P^n(\Gamma_+)$ and the pre-images $P^{-m}(\Gamma_-)$, for all $n, m \geq 2$, are similar in structure to the tongues shown in figure 7, being smooth double coverings of intervals $(\eta_n, \eta_{\text{max}})$ and $(\eta_{\text{min}}, \eta_{-m})$, respectively.

Remark 6.2. The $P^{-2}(\Gamma_-)$, $P^{-3}(\Gamma_-)$, ... tongues cannot intersect the $P^2(\Gamma_+)$, $P^3(\Gamma_+)$, ... tongues because of the fact that the flow in the η -direction is upward, since $\eta_\xi = a$ and $a > 0$. If the flow in the η -direction had not been constantly upward, then the $P^n(\Gamma_+)$ and $P^{-m}(\Gamma_-)$ tongues could have intersected, which would have led to much more complicated behaviour (see [8, 9, 16]).

6.3. The locations of segments of $W^u(\Gamma_+)$ and $W^s(\Gamma_-)$ on constant η slices

In this section, we determine the locations of long segments of the manifolds $W^u(\Gamma_+)$ and $W^s(\Gamma_-)$ on $\eta = \text{constant}$ planes for $\eta_{\min} < \eta < \eta_{\max}$ (see figure 6). We use several results, including the above information about the tongue structures of $P^n(\Gamma_+)$ and $P^{-m}(\Gamma_-)$ for $n, m \geq 1$, the fact that the manifolds are smooth, and the exchange lemma from geometric singular perturbation theory.

We begin with $W^u(\Gamma_+)$ at $\eta = \eta_{\text{zero}}$ (see figure 6(c)), and flow forward the points on that segment of $W^u(\Gamma_+)$ which lies inside of $W^s(\Gamma_-)$. There exists an $\eta_* > \eta_{\text{zero}}$ such that a point on this segment of $W^u(\Gamma_+)$ first intersects the plane $B = 0$ with $A < A_{\text{ctr}} (= \sqrt{1 - (\eta_*^2/4)})$ at $\eta = \eta_*$. In addition, there is a segment of $W_{\text{loc}}^u(\Gamma_+)$, the local part of $W^u(\Gamma_+)$, containing the transverse intersection point of $W_{\text{loc}}^u(\Gamma_+)$ and $W_{\text{loc}}^s(\Gamma_-)$ on the $\eta = \eta_{\text{zero}}$ cross section that approaches the B -axis exponentially as η increases (with the leading-order rate constant being given by the η -dependent eigenvalues of the saddle points on Γ_-) and that is C^1 close to the B -axis. Then, as η increases further past η_* , this segment is stretched out over almost the entire interval of the B -axis between the two saddles (see figure 6(e)).

Remark 6.3. Near η_{\max} , this segment of $W^u(\Gamma_+)$ lies exponentially close to the B -axis. Moreover, the width of the tongue is $\mathcal{O}(a)$ along this segment. And hence, the right boundary of this segment of the tongue is $\mathcal{O}(a)$ away from the B -axis. By a similar argument in backward time the segment of $W^s(\Gamma_-)$ that lies closest to the B -axis and that forms the left boundary of the tongue there, is exponentially close to the B -axis at $\eta = \eta_{\min}$. Finally, the right boundary of the tongue there is $\mathcal{O}(a)$ away from the B -axis. This information will be useful in section 7.

More importantly, on the cross sections of constant η , for each η sufficiently greater than η_{zero} , there is a segment of the global manifold $W^u(\Gamma_+)$ that is C^1 exponentially close to, $W_{\text{loc}}^u(\Gamma_+)$ in a neighbourhood of Γ_+ (see figure 6(e)). This C^1 closeness result follows from two applications of the exchange lemma of [18, 20, 19], interspersed with a standard estimate. For the first application of the exchange lemma, the slow manifold is the one-dimensional manifold Γ_- , which has two-dimensional stable and unstable manifolds, and the tracked manifold is a two-dimensional segment of the two-dimensional global manifold $W^u(\Gamma_+)$. The hypotheses are satisfied, since the tracked manifold transversely intersects $W_{\text{loc}}^s(\Gamma_-)$ on entry into a neighbourhood of Γ_- . Hence, the lemma allows us to conclude that, on exit from the fixed neighbourhood of Γ_- , the tracked manifold lies C^1 exponentially close to the upper branch of $W^u(\Gamma_-)$. Next, standard estimates can be used to show that the solutions on this same segment enter a neighbourhood of the other (upper) slow manifold, Γ_+ , C^1 exponentially close to the lower branch of $W_{\text{loc}}^s(\Gamma_+)$. Finally, one makes a second application of the exchange lemma, but now with Γ_+ as the slow manifold and with a modified hypothesis (the requirement that the tracked manifold transversely intersects the local stable manifold of the slow manifold is replaced by a C^1 closeness estimate on entry (see [20])). This second application leads to the conclusion that there is a segment of the global manifold $W^u(\Gamma_+)$, the tracked manifold, that is C^1 exponentially close to $W_{\text{loc}}^u(\Gamma_+)$ on exit from the neighbourhood of Γ_+ , as claimed above. Moreover, another standard estimate can be used to show that a segment of $W^u(\Gamma_+)$

containing the point r , one of the points where the tracked manifold intersects the A -axis, is also C^1 exponentially close to $W_{\text{loc}}^u(\Gamma_+)$ at r .

In conclusion, one may say that, as η increases from the value corresponding to the slice shown in figure 6(d) to that corresponding to figure 6(e), this segment of $W^u(\Gamma_+)$ curls up inside $W^s(\Gamma_-)$ in a tongue-like way (see figure 6(e)).

Remark 6.4. As a consequence of the above observations, it follows that there exists an η_{**} , satisfying $\eta_* < \eta_{**} < \eta_{\text{max}}$, such that there is a point on this segment that is the first to intersect Ω but now with $A > A_{\text{ctr}}$ at $\eta = \eta_{**}$. This intersection occurs at the point corresponding to the tip of the tongue of $P^2(\Gamma_+)$, and therefore $\eta_{**} = \eta_2$.

A similar argument shows that there is a segment of $W^s(\Gamma_-)$ that curls up inside $W^u(\Gamma_+)$ for $\eta_{\text{min}} < \eta < \eta_{\text{zero}}$ in a tongue-like way (see figure 6(a)). At $\eta = \eta_{\text{min}}$, $W^s(\Gamma_-)$ is curled up the most, and the tongue that is formed by $W^s(\Gamma_-)$ inside $W^u(\Gamma_+)$ starts to retract as η is increased. This continues up to $\eta = \eta_{\text{zero}}$, where the manifolds intersect at the B -axis (see figure 6(c)).

The extent to which $W^u(\Gamma_+)$ and $W^s(\Gamma_-)$ curl up inside themselves depends on the magnitude of a . A smaller value of a results in longer tongue structures of $W^s(\Gamma_-)$ at $\eta = \eta_{\text{min}}$ and of $W^u(\Gamma_+)$ at $\eta = \eta_{\text{max}}$, respectively. Hence, $n_0(a)$ increases as a decreases.

7. Tracking M_0 from ξ_b to ξ_{max} (i.e. from η_{min} to η_{max}) and the intersections of M^0 and M^∞ at η_{max}

In this section, we track the manifold M_0 from η_{min} to η_{max} . It will be useful to define constant η slices of M_0 . We denote these by I_η . The location of $I_{\eta_{\text{min}}}$ was already determined in section 4; $I_{\eta_{\text{min}}}$ is given by an interval around $B = -1$ that is transversal to $B = -1$, as was first shown in figure 4 and as is shown again—now with the manifolds—in figure 8(a). Moreover, the A coordinates of points located on $I_{\eta_{\text{min}}}$ are bounded in lemma 4.2 as $c_1 a^{1/2} < A_d^0(\xi_b) < c_2 a^{l_1}$ where $l > d + 1$ and $l_1 < \frac{1}{2}|B^+| \min\{(\ell - 1 - d)/2|B^-|, 1/2|B^-|\}$. Combining these bounds with the results of remark 6.3, we find that $I_{\eta_{\text{min}}}$ intersects $W^s(\Gamma_-)$ at least at the points p_1, p_2 , and p_3 as shown in figure 8(a). Also, $I_{\eta_{\text{min}}}$ intersects once with $W^u(\Gamma_+)$, in p_0 .

The points on I_η must respect the invariance properties of the manifolds $W^u(\Gamma_+)$ and $W^s(\Gamma_-)$. First, points on I_η that are also on the manifold $W^s(\Gamma_-)$, e.g. the points p_1, p_2, p_3 in figure 8(a) (which are distinct from the point p_1 in the previous section), must remain on $W^s(\Gamma_-)$ for as long as it exists. Also, points on I_η that also lie on $W^u(\Gamma_+)$, as for example the point p_0 in figure 8(a), must remain on $W^u(\Gamma_+)$. Finally, orbits that do not start on either $W^u(\Gamma_+)$ or $W^s(\Gamma_-)$ will never intersect these manifolds.

We distinguish two steps in pulling I_η forwards; step I from η_{min} to η_{zero} and step II from η_{zero} to η_{max} . In step I, the tongue structure of the manifold $W^s(\Gamma_-)$ retracts, in the manner specified in the previous section and illustrated in figures 6(a)–(c). One may say that, during this step, I_η becomes a curve that rolls up inside itself (figure 8(d)). More precisely, as η increases from η_{min} , there is a segment of I_η , which contains the point p_1 , that approaches the B -axis at an exponential rate. This segment is C^1 close to the B -axis and almost covers the entire segment of that axis between the two saddles for η sufficiently larger than η_{min} (but less than 2). In addition, there is a segment of I_η that is C^1 exponentially close to $W_{\text{loc}}^u(\Gamma_+)$ on exit of a neighbourhood of Γ_+ . This follows by applying the exchange lemma and a standard estimate in a fashion similar to the argument of the previous section. For a certain range of η values, this segment contains the points p_2 and p_3 , at which I_η and $W^s(\Gamma_-)$ transversely intersect, as shown in figure 8(c). Then, as η increases even further, the points p_2 and p_3 move

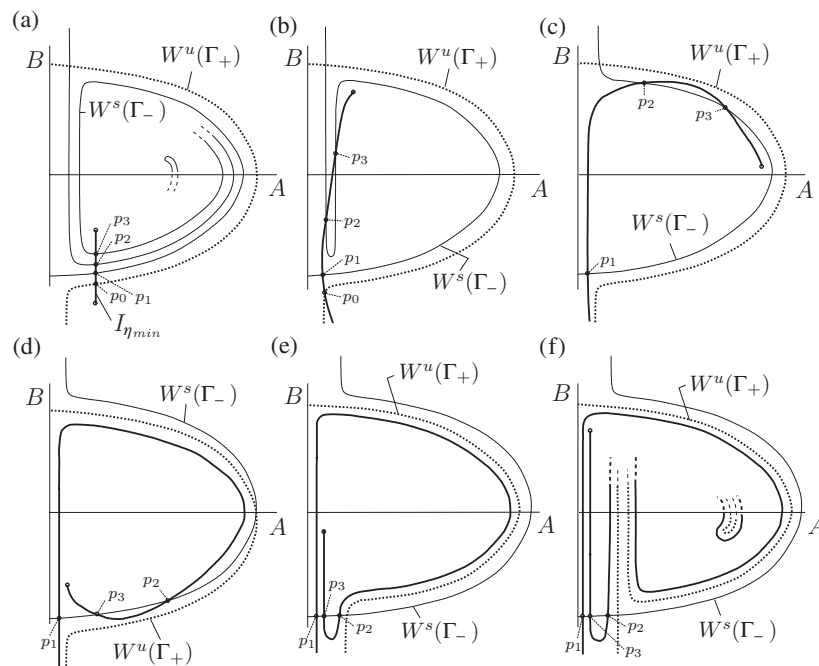


Figure 8. The transformation of I_η as η is increased from η_{\min} to η_{\max} . During this process the point p_0 remains on $W^u(\Gamma_+)$, and the points p_1, p_2 and p_3 remain on $W^s(\Gamma_-)$. (a) At $\eta = \eta_{\min}$, I_η is an interval approximately parallel to the B -axis. The smaller the value of a , the more the tongue winds around the centre point, and hence in the sketch we only denote the tip of the tongue and not all the spirals. (b)–(e) A – B planes at different values of η in step I. I_η curls up as $W^u(\Gamma_+)$ pulls back, where frame (d) is a sketch for $\eta = \eta_{\text{zero}}$. (f) At $\eta = \eta_{\max}$, I_η has formed a tongue structure as a result of the fact that $W^u(\Gamma_+)$ curls up in itself in step II.

towards Γ_- along $W^s_{\text{loc}}(\Gamma_-)$, and the segment of I_η that is C^1 close to $W^u_{\text{loc}}(\Gamma_+)$ stretches (see figure 8(d)).

In step II, $W^u(\Gamma_+)$ starts to curl up into itself like a tongue, as specified in the previous section and illustrated in figure 6(e). Since the positions of all the points on I_η with respect to $W^u(\Gamma_+)$ and $W^s(\Gamma_-)$ have to remain the same, I_η will also start to curl up into itself like a tongue (see figure 8(f)). The curve $I_{\eta_{\max}}$ has the important properties that there are segments that are C^1 exponentially close to the B -axis (namely segments containing the type L intersection points—one segment for each such point), and that there are other segments that are C^1 close to $W^u(\Gamma_+)$ (namely one segment for each of—and containing—the intersection points of type R) (see figure 9). Hence, the intersections of $I_{\eta_{\max}}$ with M^∞ are all transverse.

The structure as sketched in figure 9 is more complicated than the sketch of $I_{\eta_{\max}}$ given in figure 8(f). When constructing figure 9, we took into account that both $W^s(\Gamma_-)$ at η_{\min} and $W^u(\Gamma_+)$ at η_{\max} , for smaller values of a , wind around in the (A, B) -plane more than is sketched in figures 8(a) and (f). The fact that at η_{\min} , $W^s(\Gamma_-)$ has made more excursions around the centre point implies that there exist more intersection points of $W^s(\Gamma_-)$ and $I_{\eta_{\min}}$ than given in figure 8(a). Then, by carefully tracking I_η as η increases from η_{\min} and also taking into account that $W^u(\Gamma_+)$ winds around the centre point more than is sketched in figure 8(f), leads to the sketch in figure 9.

In summary, we have the following estimates of B and A on M^0 at ξ_{\max} , where we denote these values by $B^0(\xi_{\max})$ and $A^0(\xi_{\max})$.

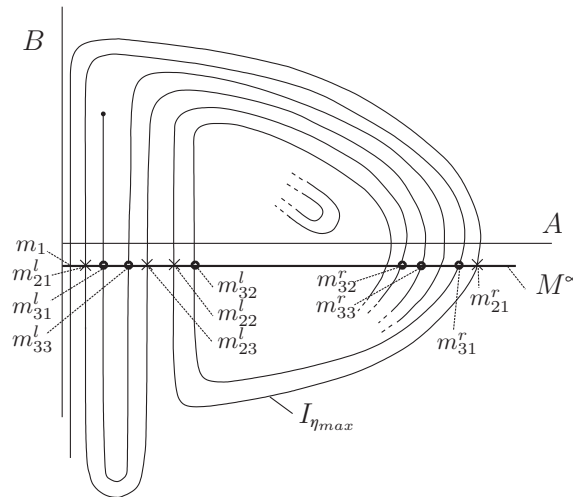


Figure 9. A schematic of M^∞ and I_η at $\eta = \eta_{\max}$ in the A - B plane. At the intersection point m_{11}^l of M^∞ and I_η the monotonically decreasing solution is found. At the points marked by a cross, the m_{2i}^r and m_{2i}^l 2-bump solutions are formed for $i = 1, 2, 3$. At the points marked by a dot, the m_{3i}^r and m_{3j}^l 3-bumps solutions occur for $i, j = 1, 2, 3$. The existence of all these intersection points is demonstrated in section 7. Please note that only some of the intersection points that form a 3-bump solution are sketched here, to maintain clarity in this figure.

Lemma 7.1. For points on the curve I_η at $\xi = \xi_{\max}$, the values of $B^0(\xi_{\max})$ are mapped onto the interval $(-a^{1/4} + \frac{1}{8}a^{3/4}, a^{1/4} - \frac{1}{8}a^{3/4})$.

Proof. At $\eta = \eta_{\max}$, the value of B on the heteroclinic orbit (5.4) of the unperturbed system varies between $-\sqrt{1 - (\eta_{\max}^2/4)}$ and $\sqrt{1 - (\eta_{\max}^2/4)} = a^{1/4}\sqrt{1 - \frac{1}{4}\sqrt{a}} = a^{1/4} - \frac{1}{8}a^{3/4} + \text{hot}$. Since parts of the curve $I_{\eta_{\max}}$ lie $\mathcal{O}(a)$ close to this heteroclinic orbit and other parts lie exponentially close to the B -axis, we conclude that the B -values on $I_{\eta_{\max}}$ are mapped onto the interval $(-a^{1/4} + \frac{1}{8}a^{3/4}, a^{1/4} - \frac{1}{8}a^{3/4})$. \square

Combining this result with the estimate obtained in lemma 3.2, $B_d^\infty(\xi_{\max}) = -a^{1/4} + c_1\sqrt{a}$, one finds that there are solutions on M^0 and M^∞ such that the B coordinates of these solutions overlap at ξ_{\max} .

We also have the following estimate for $A^0(\xi_{\max})$.

Lemma 7.2. The intersection points of the curve I_η and the line $B_d^\infty(\xi_{\max}) = -a^{1/4} + c_1\sqrt{a}$ can be split into two groups. One group of points lies close to the heteroclinic orbit (5.4) of the unperturbed problem, (2.8) with $a = 0$ and $\eta = \eta_{\max}$. For these points, $A^0(\xi_{\max}) = 2\sqrt{c_1}a^{3/8} - ((c_1^2 + 1/4)/2\sqrt{c_1})a^{5/8} + \text{hot}$, and we label these as points of type R. For the other intersection points, $A^0(\xi_{\max})$ is exponentially small, and we label them as points of type L. Hence, the A coordinates of all intersection points lie in the interval $(0, 2\sqrt{c_1}a^{3/8})$.

Proof. We start by determining the A values of the intersection points that lie close to the heteroclinic orbit (5.4) of the unperturbed problem, (2.8) with $a = 0$ and $\eta = \eta_{\max}$. We know that segments of the curve I_η at $\eta = \eta_{\max}$ lie a distance c_2a away from this heteroclinic orbit. For the heteroclinic orbit, $\kappa_1 \equiv 0$, where κ_1 is defined in (6.1) as $\kappa_1 = \frac{1}{2}A^2B^2 - \frac{1}{2}(1 - (\eta^2/4))A^2 + \frac{1}{4}A^4$. Substituting $B = -a^{1/4} + c_1\sqrt{a}$ into $\kappa_1 = 0$,

together with $\eta = \eta_{\max} = 2 - \sqrt{a}$, we find $A = 2\sqrt{c_1}a^{3/8} - ((c_1^2 + 1/4)/2\sqrt{c_1})a^{5/8} + \text{hot}$ for the A values of these intersection points. For the other points, A lies close to 0, $A^0(\xi_{\max})$ is even exponentially small. Thus, for all the intersection points we find $0 < A^0(\xi_{\max}) < 2\sqrt{c_1}a^{3/8}$. \square

Hence, there are solutions on M^0 and M^∞ for which the A coordinates coincide at η_{\max} , since we saw from section 3 that $A_d^\infty(\xi_{\max})$ is onto $[0, a^{3/8}]$ as a function of $A_1 = A(\sqrt{2}/a\sqrt{a})$.

Therefore, we find by putting these results together that there are solutions on M^0 and M^∞ for which the A and B coordinates at ξ_{\max} are the same. Moreover, the manifolds M^0 and M^∞ intersect transversely in the A - B plane at $\xi = \xi_{\max}$, as follows from combining lemma 3.5, which states that M^∞ is C^1 close to the line $B_d^\infty(\xi_{\max}) = -a^{1/4} + c_1\sqrt{a}$, and the above tracking arguments for M^0 .

The above results are almost enough to prove theorem 2.1. There are three outstanding issues. First, we need to show that the assumption on ϕ that we made above, namely that $|\phi| < a$ for $\xi \leq \xi_{\max}$, is satisfied. This is proved in section 8. Second, we need to extract some more quantitative information about the full solutions that lie in the transverse intersections of M^0 and M^∞ , such as locations of local maxima and distances between them, as stated in the theorem. This is done in section 9. Third, it is critical to observe that, while solutions can be chosen so that the A and B coordinates are the same at $\xi = \xi_{\max}$, it is not necessarily the case that the ψ coordinates of these solutions also agree. Therefore, in section 10, we analyse the dynamics of the ψ coordinate. We show that for each of the distinct intersection points found above there is a locally unique d (near 2) such that the ψ coordinates also coincide. This completes the proof of the desired result that the three-dimensional manifolds M^0 and M^∞ have two families of transverse intersection points in the $A - B - \psi - \xi - d$, extended, five-dimensional phase space and, hence, that the locally unique, multi-bump solutions claimed in theorem 2.1 exist, with the properties stated there.

Remark 7.1. The point p_0 disappears in figure 8(c), since it moves down (out of the figure).

Remark 7.2. As was already noted in remark 3.1, we can use a more general setting and pull back M^∞ to a point $\xi = (2 - b)/a$ where $a^{2/3} \ll b \ll a^{2/5}$. This can be done as follows: at $\eta = 2 - b$, the constant η slice of M_0 lies exponentially close to the heteroclinic orbit that exists for $a = 0$. Thus, to make sure that M^0 and M^∞ intersect, we must have that the projection of M^∞ at $\xi = \xi_{\max}$ lies within this heteroclinic orbit. This is satisfied when $B_d^\infty(\xi_{\max}) \gg -\sqrt{1 - (\eta_{\max}^2/4)}$ and this leads to the condition $b \ll a^{2/5}$. The $a^{2/3}$ boundary is needed to ensure that the higher order terms in $B(\eta = 2 - b)$ are really of higher order (see also remark A.1 in appendix A in the proof of lemma 3.1). A different choice of η_{\max} would of course also influence other estimates, for example, lemma 7.2 concerning the estimates of A at $\xi = \xi_{\max}$ in the multi-bump region.

8. The bound on ϕ

In the foregoing tracking analysis, we assumed that $|\phi| < a$ for $\xi \leq \xi_{\max}$. We now turn to prove this statement. We begin with lemma 5.2 from [35].

Lemma 8.1. *A solution that satisfies the initial conditions $B(0) = 0$ and $\phi(0) = 0$, i.e. $\psi(0) = 0$, can be represented as*

$$\phi(\xi) = \psi(\xi) + \frac{a\xi}{2} = \frac{a\xi^{1-d}}{2A^2(\xi)}(d-2) \int_0^\xi A^2(x)x^{d-1} dx. \quad (8.1)$$

Proof. We define

$$M(x) = A^2(x)x \left(\psi(x) + \frac{ax}{2} \right).$$

Then

$$\begin{aligned} \frac{d}{dx}(x^{d-2}M) &= x^{d-2} \left[xA^2\psi_x + 2xA A_x \left(\psi + \frac{ax}{2} \right) + A^2 \left((d-1)\psi + \frac{adx}{2} \right) \right] \\ &= (d-2) \frac{ax^{d-1}}{2} A^2. \end{aligned}$$

For the second equality, the equations that are known for A_x and ψ_x in system (2.5) were substituted. Integrating from 0 to ξ and substituting the definition of M , we find the statement of the lemma. \square

The explicit expression (8.1) for ϕ from the previous lemma enables us to approximate ϕ for $\xi \leq \xi_{\max}$ as follows.

Lemma 8.2. *There exists a positive constant $C > 0$ such that, for $\ell > d + 1$, $0 < k_b < (l - d - 1)/2|B^-|$, $0 < a \ll 1$, and $d - 2 = \mathcal{O}(a^\ell)$, we have that $\phi(\xi) < Ca$ for every $\tau \leq \xi \leq \xi_{\max}$.*

The proof of this lemma is given in appendix C, and it is also based on continuous induction.

9. The intersections of M^0 and M^∞ at $\eta = \eta_{\max}$

In lemma 7.2, we showed that the intersection points of M^0 and M^∞ can be split into two types, L and R. We now label the intersection points m_{ij}^l and m_{ij}^r , where $i, j \in \mathbf{N}$, corresponding to points of type L and R, respectively, with the superscript corresponding to the type of the intersection point and with the index i denoting the number of maxima of the solution. Moreover, the monotonically decreasing solution studied in [35] is found again, i.e. the point m_{11}^l results in the existence of this 1-bump solution; it has one maximum at $\xi = 0$.

The number of maxima of a solution is determined by the number of times I_η winds around the centre point in the A - B plane as η increases from η_{\min} to η_{\max} , and this number increases as a decreases. Each time I_η crosses the A -axis through the cross section Ω , an extra maximum is added. Thus, by carefully keeping track of the number of these crossings, one can determine the number of maxima of a solution corresponding to an intersection point. An n -bump solution will consist of a maximum in $\xi = 0$ and $n - 1$ local maxima, and the values of η where these maxima occur are all smaller than η_{\max} .

9.1. The 2-bump solutions

We will start by describing the 2-bump solutions that correspond to the four intersection points labelled $m_{21}^r, m_{21}^l, m_{22}^l, m_{23}^l$ in figure 9. We do this by keeping track of I_η as η increases from η_{\min} to η_{\max} . As I_η curls up inside itself in step I in the manner specified in the previous section, I_η crosses the A -axis once close to A_{\max} , whereas in step II it does not. Thus, one maximum is formed apart from the maximum at $\xi = 0$.

There is a qualitative difference between the solution that is constructed at m_{21}^r and the ones at the points m_{2i}^l . This difference stems from the difference in type, R or L, of the solution, i.e. what the value of $A(\eta_{\max})$ is at the intersection of M^0 and M^∞ . The last maximum of the solution (in this case the second) will be reached at a different value of η for the two different types of solutions. The last maximum of the 2-bump solution corresponding to m_{21}^r is reached

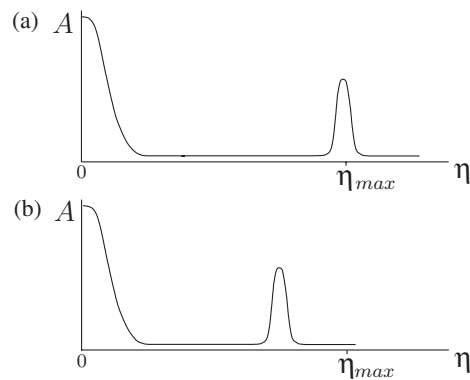


Figure 10. A sketch of the different types of 2-bump solutions: (a) the solution of type R created at m_{21}^r ; (b) the three solutions of type L, which are exponentially close to each other and hence indistinguishable in this sketch, correspond to the three intersection points m_{2i}^l , $i = 1, 2, 3$.

for η close to η_{\max} ; therefore, at this maximum $A = \sqrt{2(1 - (\eta_{\max}^2/4))} = \sqrt{2}a^{1/4}(1 - \frac{1}{8}\sqrt{a})$ to leading order. Thus, $A(\eta_{\max}) = A_{\max} + c_2 a$ for some constant c_2 (see figure 10(a) for a sketch of this 2-bump). For the 2-bumps corresponding to the points m_{2i}^l , $i = 1, 2, 3$, $A(\eta_{\max})$ is exponentially small. Thus, the second maximum is reached well before $\eta = \eta_{\max}$ (see figure 10(b)). Also, the points m_{2i}^l all lie exponentially close to each other for $\eta > \eta_{\text{zero}}$; therefore, the three solutions of type L also lie exponentially close to each other.

9.2. The construction of n -bump solutions for $n \geq 2$

Following the method used above to construct 2-bump solutions, we now show that there exist solutions with n local maxima for each $n \geq 2$. The number of n -bump solutions can be determined explicitly (for a sufficiently small), where again a qualitative difference occurs between solutions of type R and of type L, as stated in theorem 2.1.

For $n = 2$, we proved in the previous section the existence of four 2-bump solutions, one of type R and three of type L. We continue the argument for more general n , starting with $n = 3$, by again studying the intersection of M^0 and M^∞ at η_{\max} (for a sufficiently small). As a decreases, the stable and unstable manifolds $W^u(\Gamma_+)$ and $W^s(\Gamma_-)$ curl up more into themselves which implies that I_η also curls up more into itself. More precisely, comparing $W^s(\Gamma_-)$ for $a = a_0$ to $a = a_1$, where $0 < a_1 < a_0 \ll 1$, it is curled up more at $\eta = \eta_{\min}$ for a_1 than for a_0 . A similar statement holds for $W^u(\Gamma_+)$ at $\eta = \eta_{\max}$. Therefore, when we follow I_η as η increases from η_{\min} to η_{\max} we find, using the two steps distinguished in section 7, that there exist more intersection points of M^0 and M^∞ at η_{\max} besides the points leading to 2-bumps (see also figure 9). Also, the number of times that one crosses the A -axis near A_{\max} to reach such an intersection point increases and therefore, the number of local maxima of a solution increases.

First, we focus on the 3-bump solutions that are formed in a similar way as the 2-bumps. In step I of the transformation of I_η , as it winds around the A - B plane, a segment of I_η has intersected with the A -axis twice at A_{\max} , which results in the construction of 3-bump solutions at the points m_{31}^r and m_{31}^l (see figure 9). In step II where I_η forms a tongue, this same part of I_η will again intersect with M^∞ this time exponentially close to 0. These intersection points, m_{32}^l and m_{33}^l (see figure 9), correspond to a pair of 3-bump solutions of type L. So far, the

solutions are all constructed in a similar way as the 2-bump solutions. However, more 3-bump solutions are formed in step II. These are constructed from the tongue-like branch on which the points m_{22}^l and m_{23}^l lie. This branch winds around the A - B plane to intersect once again with the A -axis close to A_{\max} and, therefore, when it intersects with M^∞ at m_{32}^r and m_{33}^r two extra 3-bump solutions of type R are formed. These solutions have an extra maximum compared to the solutions at the points m_{22}^l and m_{23}^l and therefore form 3-bump solutions. As I_η curls up further (for a sufficiently small), this branch will again intersect with M^∞ exponentially close to $A = 0$, at m_{34}^l and m_{35}^l , to give two extra 3-bump solutions of type L. Thus, for a sufficiently small, there exist eight 3-bump solutions, three of which are of type R and five of type L. Finally, the points m_{3i}^l all lie exponentially close to each other.

The number of 3-bump solutions follows easily from the number of 2-bump solutions. One 3-bump solution of type R and three 3-bump solutions of type L are formed in a similar way as the 2-bumps. Besides these, two extra 3-bumps of type R and two of type L are formed on the branches where the 2-bump solutions occur. Thus, the number of 3-bumps of type L increases by 2 with respect to the number of 2-bumps of type L, and the same holds for the number of 3-bumps of type R.

Inductively, the $(n + 1)$ -bump solutions can be formed from the n -bumps, and the number of $(n + 1)$ -bumps also follows from the number of n -bumps, as long as $n + 1 \leq n_0(a)$ for the given, sufficiently small, value of a . The number of solutions of both types L and R increases by two as the number of local maxima increases from n to $n + 1$.

10. Matching the ψ coordinate

So far, we showed that on the cross section $\xi = \xi_{\max}$ there exist two families of solutions on M^0 and M^∞ for which the A and B coordinates are the same (for a sufficiently small). In this section, we will show that d can be chosen such that the ψ coordinate of M^0 and M^∞ are the same; and, hence, the proof of theorem 2.1 will be complete. The analysis of the ψ coordinate consists of two parts. First, we show that, at $\xi = \xi_{\max}$, the interval of possible values of ψ on M^0 overlaps the interval of possible values on M^∞ . We showed in section 3 that the distance between $\psi_d^\infty(\xi_{\max})$ and $-a\xi_{\max}/2$ is exponentially small (see lemma 3.2). Therefore, to ensure that the intervals of the possible values of ψ on M^0 and on M^∞ overlap, it is sufficient to show that the distance between $\psi_d^0(\xi_{\max})$ and $-a\xi_{\max}/2$ is larger than exponentially small, for a range of d values. Then, we will show that the intersection is transversal so that d can be chosen such that $\psi_d^\infty(\xi_{\max})$ and $\psi_d^0(\xi_{\max})$ match (see figure 11).

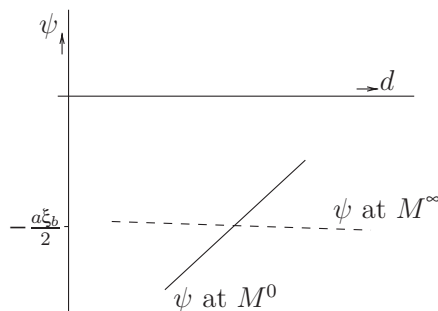


Figure 11. A sketch of the ψ coordinates of the manifolds M^0 (—) and M^∞ (- - -) at $\xi = \xi_{\max}$ as a function of d .

10.1. Overlap of the ψ intervals

First, we show that $|\psi_d^0(\xi_{\max}) + a\xi_{\max}/2|$ is larger than an exponentially small term in a . We can get a lower bound from the expression (8.1). Since A is strictly positive, we have that $\int_0^{\xi} A^2(x)x^{d-1}dx > \hat{K} > 0$. Then, using the fact that the solution at ξ_{\max} lies $\mathcal{O}(a)$ close to the heteroclinic orbit, we have that $A(\xi_{\max}) < \sqrt{2a}$, and therefore $1/A(\xi_{\max})^2 \geq 1/2a$.

Thus, expression (8.1) gives

$$\left| \psi_d^0(\xi_b) + \frac{a\xi_{\max}}{2} \right| > \tilde{c}\xi_{\max}^{1-d}(d-2) = c_1a(d-2). \quad (10.1)$$

This implies that, as we vary d , the interval of values of $\psi_d^0(\xi_{\max})$ overlaps the interval of values of $\psi_d^\infty(\xi_{\max})$.

10.2. The transversal intersection

Here, we show that there exists a locally unique value of d for which $\psi_d^0(\xi_{\max}) = \psi_d^\infty(\xi_{\max})$. Specifically, we prove that the intersection of $\psi_d^0(\xi_{\max})$ and $\psi_d^\infty(\xi_{\max})$, as functions of d , is transversal by examining the derivatives of $\psi_d^\infty(\xi_{\max})$ and $\psi_d^0(\xi_{\max})$ with respect to $\Delta = d-2$. It follows, from lemma 3.2, that $\psi_d^\infty(\xi_{\max}) + a\xi_{\max}/2$ is exponentially small. This immediately gives that

$$\frac{\partial \psi_d^\infty(\xi_{\max})}{\partial \Delta} \leq e^{-c/a} \quad (10.2)$$

for some positive constant c . Now, we will show that the derivative of $\psi_d^0(\xi_{\max})$ with respect to Δ is larger than an exponentially small term.

Lemma 10.1. *There exists a constant $c_1 > 0$ such that $\partial \psi_d^0 \xi_{\max} / \partial \Delta \geq c_1 a$.*

Proof. Differentiating expression (8.1) with respect to Δ leads to

$$\begin{aligned} \frac{\partial \psi_d^0(\xi_{\max})}{\partial \Delta} &= \frac{a\xi_{\max}^{1-d}}{2A^2} \int_0^{\xi_{\max}} A^2 x^{d-1} dx + \xi_{\max}^{1-d} \log \xi_{\max}^{-1} \frac{a}{2A^2} (d-2) \int_0^{\xi_{\max}} A^2 x^{d-1} dx \\ &\quad + \frac{a\xi_{\max}^{1-d}}{2A^2} (d-2) \int_0^{\xi_{\max}} (\log x) A^2 x^{d-1} dx + \frac{a\xi_{\max}^{1-d}}{2A^2} (d-2) \int_0^{\xi_{\max}} \frac{2}{A} \frac{dA}{d\Delta} A^2 x^{d-1} dx \\ &\quad - \frac{a\xi_{\max}^{1-d}}{A^2} (d-2) \frac{1}{A} \frac{dA}{d\Delta} \int_0^{\xi_{\max}} A^2 x^{d-1} dx \\ &= I_1 + I_2 + I_3 + I_4 + I_5. \end{aligned} \quad (10.3)$$

We will show that the first term I_1 is much larger than the other terms. Note that from the expression for ψ (8.1) it follows that $I_1 = (1/(d-2))(\psi_d^0(\xi_{\max}) + a\xi_{\max}/2)$. So, from the approximation (10.1) we have $I_1 > c_1 a$. The integral I_2 can be approximated because $|I_2| = |\log \xi_{\max}(d-2)I_1| \ll a^{-p}(d-2)I_1$ for every $p > 0$, where we use the fact that $\log \xi_{\max} \ll a^{-p}$ for every $p > 0$ and $a \ll 1$. Recall that we set $d-2 = \mathcal{O}(a^\ell)$, where $\ell > 0$ is arbitrary. The choice $p = \ell$ implies that $|I_2| \ll I_1$. To study I_3 , we approximate the integral

$$\int_0^{\xi_{\max}} (\log x) A^2 x^{d-1} dx \leq \log \xi_{\max} \int_0^{\xi_{\max}} A^2 x^{d-1} dx.$$

So, $I_3 \leq (\log \xi_{\max})(d-2)I_1$; hence, I_3 is much smaller than I_1 , just as I_2 is much smaller than I_1 . To determine I_4 and I_5 , we must study $(1/A)(dA/d\Delta)$. We will show in appendix D that $(1/A)(dA/d\Delta) \leq ca^{|B^-|k_b+1/2}$ for $0 < \xi < \xi_{\max}$. Here, $k_b > 0$ is introduced in $\xi_b = k_b \log(1/a)$ and can still be chosen. Using this, we find that $|I_4| \leq 2(d-2)ca^{B^-k_b+1/2}I_1 \ll I_1$

for $0 < k_b < (1 + 2\ell)/2|B^-|$. Finally, $|I_5| \ll I_1$ as may be shown in a similar way as for I_4 . Thus, I_1 is much larger than the other terms and hence $\partial\psi_d^0(\xi_{\max})/\partial\Delta > I_1 > c_1a$. \square

The above lemma implies that $\partial\psi_d^0(\xi_{\max})/\partial\Delta \gg \partial\psi_d^\infty(\xi_{\max})/\partial\Delta$ (see figure 11). Therefore, the intersection of $\psi_d^0(\xi_{\max})$ and $\psi_d^\infty(\xi_{\max})$ at $\xi = \xi_{\max}$ is transverse, which implies that there exists a unique d such that $\psi_d^0(\xi_{\max}) = \psi_d^\infty(\xi_{\max})$.

Acknowledgments

We thank Nancy Kopell for useful conversations. We also thank Arjen Doelman and Chris Budd for their thorough reading of this paper. We are also grateful to Arjen for finding an insufficiently sharp estimate in the initial presentation and Chris for sharing his results in [2] about the asymptotics of multi-bump solutions prior to publication, as well as for stimulating conversations and his permission to use a figure from [2], which is reproduced here as figure 1. The work of VR has been made possible by a fellowship of the Royal Netherlands Academy of Arts and Sciences and was partially supported by the Dutch Science Organization and by the RTN network ‘Nonlinear Partial Differential Equations describing Front Propagation and other Singular Phenomena’, HPRN-CT-2002-00274. The work of TK was partially supported by the NSF grant DMS-0072596.

Appendix A. The proof of lemma 3.1

To prove the estimates for B and ψ given in lemma 3.1, we study the leading order equation (3.3) for W . This is done along the same lines as in [36]. Introducing the rescaling $\eta = a\xi$ into (3.3) leads to

$$a^2W_{\eta\eta} + W \left[\frac{\eta^2}{4} - 1 \right] = 0. \tag{A.1}$$

To analyse this equation close to the turning point $\eta = 2$, we introduce the new variable $\zeta = 2(1 - (\eta/2))a^{-2/3}$, i.e. $\eta = 2 - \zeta a^{2/3}$. Then, (A.1) reduces to the Airy equation

$$W_{\zeta\zeta} - \zeta W = 0,$$

as long as $\frac{1}{4}\zeta a^{23} \ll 1$. The general solution $W = k_1\text{Ai}(\zeta) + k_2\text{Bi}(\zeta)$ to this equation can be approximated in the limit $\zeta \rightarrow \infty$, or equivalently $\eta \uparrow 2$ with the condition $\eta \ll 2 - a^{23}$, by

$$W(\eta) = \frac{a^{1/6}}{\sqrt{\pi}2^{1/4}(1 - \eta/2)^{1/4}} \left\{ \frac{1}{2}k_1 \exp \left[-\frac{4\sqrt{2}}{3a} \left(1 - \frac{\eta}{2}\right)^{3/2} \right] + k_2 \exp \left[\frac{4\sqrt{2}}{3a} \left(1 - \frac{\eta}{2}\right)^{3/2} \right] \right\}.$$

Now, if $\eta > 2$, the Airy function solution for $\zeta \rightarrow -\infty$ is asymptotic to

$$W(\eta) \sim \frac{a^{1/6}}{2\sqrt{\pi}((\eta/2) - 1)^{1/4}} \left\{ k_1 \sin \left(2\sqrt{2} \left(\frac{\eta}{2} - 1 \right)^{3/2} + \frac{\pi}{4} \right) + k_2 \cos \left(2\sqrt{2} \left(\frac{\eta}{2} - 1 \right)^{3/2} + \frac{\pi}{4} \right) \right\}. \tag{A.2}$$

However, for large η , $|W|$ must be monotonically decreasing (i.e. there can be no oscillations in the amplitude of W), and this is only true for (A.2) if $k_1 = \pm ik_2$. We choose $k_1 = ik_2$ following [36].

We return to the limit in which $\zeta \rightarrow \infty$, and we approximate B and ψ : using the relations (3.5) between B , ψ , and W :

$$B = \operatorname{Re} \left(\frac{W_\xi}{W} \right) + \frac{1-d}{2\xi},$$

$$\psi = \operatorname{Im} \left(\frac{W_\xi}{W} \right) - \frac{a\xi}{2}.$$

Hence, we find

$$B(\eta) = \frac{a}{8(1-(\eta/2))} - \sqrt{2} \left(1 - \frac{\eta}{2} \right)^{(1/2)} + \frac{a(1-d)}{2\eta} + \text{hot}$$

for η close to 2 but $\eta \ll 2 - a^{2/3}$, i.e. $\zeta \rightarrow \infty$. Hence,

$$B(\eta_{\max}) = -a^{1/4} + \frac{1}{4}\sqrt{a} + \text{hot}.$$

It can be shown in a similar way that ψ at η_{\max} is given to leading order by

$$\psi(\eta_{\max}) = \frac{-\eta_{\max}}{2} + a^{1/4} e^{-(4/3)a^{-1/4}}.$$

These are the estimates stated in lemma 3.1. Moreover, if $k_1 = -ik_2$ is chosen instead, then $\psi(\eta_{\max}) + (\eta_{\max}/2)$ is also exponentially small.

Remark A.1. It follows, from the above calculation, that η_{\max} can be chosen more generally as $\eta_{\max} = 2 - b$, as long as $b \gg a^{2/3}$. This would give a more general statement as noted in remark 3.1.

Appendix B. The proof of lemma 3.3

Here, we will prove lemma 3.3 using the construction we explained in section 3. First, assume that $y(\xi)$ is exponentially small for $\xi \geq \xi_2$. In a similar way as in the proof of lemma 3.1, we may use an integrating factor in (3.9) and estimate to show that \hat{z} and $\hat{\phi}$ stay exponentially small for $\xi \geq \xi_2$.

The first equation of (3.9) can be written as $y_\xi = (\bar{z} + \hat{z})y$. If we assume that \hat{z} is exponentially small, the rate of growth of y , integrated backwards from ξ_1 , is governed by \bar{z} . Then, the use of an integrating factor shows that y stays exponentially small for $\xi \geq \xi_2$ if $y(\xi_1)$ is chosen sufficiently small. We restrict to those solutions for which $y(\xi_1)$ is such that $y(\xi)$ stays exponentially small for $\xi \geq \xi_2$. Then, combining these two statements, we can conclude that the solutions satisfy the first property of the space \mathcal{V} .

Next, we focus on property (b). Rewrite the $(\hat{z}, \hat{\phi})$ -system as one equation for the complex scalar $\hat{z} + i\hat{\phi}$. If we assume that $|y| < 2a^{-1/8}$, then \hat{z} can be estimated by the non-homogeneous term $-\frac{1}{2}a^{-1/4}\xi^{1-d}y^2$ (by using an integrating factor) so $|\hat{z}| < \sqrt{a}$ for $\xi \geq \xi_{\max}$. However, there is no imaginary part in this term; thus, $\hat{\phi}$ can be approximated by the imaginary part of the linear factor $-\bar{z} + 2i\hat{\phi}$. Since $\bar{\phi}$ is exponentially small we find the same for $\hat{\phi}$. The above argument gives that $|\hat{z}| < \sqrt{a}$ and $\hat{\phi}$ is exponentially small for $\xi \geq \xi_{\max}$.

Finally, we assume that $|\hat{z}| < \sqrt{a}$. Again, by $y_\xi = (\bar{z} + \hat{z})y$, the rate of expansion of y is governed essentially by estimates on \bar{z} . We know that \bar{z} approaches $-a^{1/4}$ over a substantial portion of the interval $\xi_{\max} \leq \xi \leq \xi_2$. Therefore, we can choose a subinterval of the parameter range for $y(\xi)$ with $y(\xi_2)$ exponentially small so that, for each $y(\xi_1)$ in that interval, we have $y(\xi) < 2a^{-1/8}$ for all $\xi \geq \xi_{\max}$. This concludes the proof of the second property of the space, and from this the statement in the lemma follows.

Appendix C. The proof of lemma 8.2

This estimate was already proved in lemma 5.3 in [35] for $\tau < \xi \leq \xi_b$. Therefore, we now focus on values of ξ where $\xi_b < \xi \leq \xi_{\max}$. We will use the expression (8.1) for ϕ given in lemma 8.1 and bound the two A -dependent terms. Assuming that $\xi_b < \xi \leq \xi_{\max}$, we can split the integral in (8.1) into two parts:

$$\int_0^\xi A^2(x)x^{d-1} dx = \int_0^{\xi_b} A^2(x)x^{d-1} dx + \int_{\xi_b}^\xi A^2(x)x^{d-1} dx.$$

Lemma 4.1 gives an interval of initial conditions such that all the trajectories with these initial conditions satisfy $B^- < B(\xi) < B^+$ for all $\tau \leq \xi \leq \xi_b$. For these trajectories, one can prove that there exists a positive constant C_1 , that depends on τ , such that

$$\int_0^{\xi_b} A^2(x)x^{d-1} dx < C_1$$

(see [35]). The second integral can be bounded by using the fact that the solution constructed in sections 5.1 to 9 lies $\mathcal{O}(a)$ from the heteroclinic orbit of the unperturbed system, (2.8) with, $a = 0$. Hence, recalling (5.4), we find that $0 < A(\xi) \leq \sqrt{2(1 - (a^2\xi^2/4))} + \mathcal{O}(a)$ for all $\xi_b < \xi \leq \xi_{\max}$. Therefore,

$$\begin{aligned} \int_{\xi_b}^\xi A^2(x)x^{d-1} dx &\leq 2 \int_{\xi_b}^\xi \left(1 - \frac{a^2x^2}{4}\right) x^{d-1} dx \\ &\leq 4a^{-d} + \text{hot}, \end{aligned} \tag{C.1}$$

where $\xi \leq \xi_{\max}$. Combining these two results, we can bound the integral in expression (8.1) by c_5a^{-d} to leading order for some positive constant c_5 .

Now, we focus on the $1/(A^2(\xi))$ term. It follows from $A_\xi = AB$ and the use of an integrating factor that

$$A(\xi) = A(\xi_b) \exp \left[\int_{\xi_b}^\xi B ds \right] \tag{C.2}$$

for every $\xi_b < \xi \leq \xi_{\max}$. We use the fact that B lies $\mathcal{O}(a)$ close to the periodic solution $B^{(k)}$, (5.6), of the unperturbed system where $k \rightarrow 1$. We denote the first intersection point of the solution with $B = 0$ by ξ_3 and split the integral into two parts. Note that at this intersection point, $A < \alpha$. Combining the fact that the integration of the periodic solution $B^{(k)}$ over one whole period leads to no contribution in the integral together with the fact that B is positive just to the right of ξ_3 , we find that

$$\int_{\xi_3}^\xi B ds \geq 0 + \mathcal{O}(a)$$

for $\xi_3 < \xi \leq \xi_{\max}$. Note that this is analogous to the statement that $\int_0^x \sin(s) ds \geq 0$ for $x \geq 0$. It remains to bound the integral of B from ξ_b to ξ_3 . Now, since $B < 0$ for $0 < \xi < \frac{1}{2}T_0^{(k)}$ and $[\xi_b, \xi_3] \subset [0, \frac{1}{2}T_0^{(k)}]$, we find that

$$\int_{\xi_b}^{\xi_3} B ds \geq \int_0^{(1/2)T_0^{(k)}} B^{(k)}(s) ds + \mathcal{O}(a)$$

as $k \rightarrow 1$, where $T_0^{(k)}$ is the period of $B^{(k)}$. This integral, which is negative, can be calculated, since we know an explicit expression (5.6) for $B^{(k)}$. Using the relations between the Jacobi

elliptic function (see, e.g. [4]), we find that

$$\int_0^{(1/2)T_0^{(k)}} B^{(k)}(s) ds = \log \left(\operatorname{dn} \left(\frac{1}{2} \beta T_0^{(k)}, k \right) \right) - \log(\operatorname{dn}(0), k) = \log(\sqrt{1-k^2}).$$

Here, the expression for $T_0^{(k)}$ from section 5.1 was substituted.

Now, we must determine in more detail how k depends on a . So far, it is only known that $k \rightarrow 1$ for the solutions we are studying. Substituting the expressions (5.5) and (5.6) for the periodic solutions $(A^{(k)}(\xi), B^{(k)}(\xi))$ of the unperturbed system into the integral κ_1 (6.1), we obtain

$$\kappa_1 = \alpha^4 \frac{k^2 - 1}{(2 - k^2)^2}. \quad (\text{C.3})$$

The fact that the solution we constructed lies $\mathcal{O}(a)$ close to the heteroclinic solution then enables one to conclude that it crosses the A -axis at $(A, B) = (\sqrt{2}\alpha - ca, 0)$ for some positive constant c . Substituting this into expression (6.1) for κ_1 , one derives

$$\kappa_1 = -\sqrt{2}ca\alpha^3 + \mathcal{O}(a^2). \quad (\text{C.4})$$

Equating the two expressions (C.3) and (C.4) for κ_1 and assuming that k lies close to 1, we then see that, to leading order,

$$k = 1 - \frac{ca}{\sqrt{2}\alpha}, \quad (\text{C.5})$$

where $c > 0$. Therefore,

$$\log(\sqrt{1-k^2}) = \frac{1}{2} \log \left(\frac{\sqrt{2}}{\alpha} ca \right) + \text{hot} \geq \frac{1}{2} \log(\sqrt{2}ca) = \frac{1}{2} \log a + \text{hot},$$

where we use the fact that $\eta \geq \eta_{\min}$ and $\alpha = \sqrt{1 - (\eta^2/4)}$. Note that this term is negative. Therefore,

$$\int_{\xi_b}^{\xi} B ds \geq \frac{1}{2} \log(a) + \text{hot}$$

for every $\xi_b \leq \xi \leq \xi_{\max}$. Thus, using (C.2), one finds that there exists a positive constant c_1 such that

$$A(\xi) \geq A(\xi_b)a^{1/2} + \text{hot}$$

for every $\xi_b \leq \xi \leq \xi_{\max}$. The factor $A(\xi_b)$ can be approximated, since $B > B^-$ for $\tau \leq \xi \leq \xi_b$, as follows:

$$A(\xi_b) = A(\tau) \exp \left[\int_{\tau}^{\xi_b} B ds \right] \geq c e^{B^- \xi_b} = c \exp \left(B^- k_b \log \left(\frac{1}{a} \right) \right) = ca^{-B^- k_b},$$

for some positive constant c . Therefore, there exists a positive constant c_3 such that

$$\frac{1}{A^2(\xi)} \leq c_3 a^{2B^- k_b - 1} \quad (\text{C.6})$$

for $\xi_b \leq \xi \leq \xi_{\max}$.

Now, we can bound ϕ for $\xi_b \leq \xi \leq \xi_{\max}$ by substituting (C.1) and (C.6) into expression (8.1),

$$\begin{aligned} |\phi(\xi)| &\leq \tilde{c} \xi_b^{1-d} (d-2) a^{-d+2B^- k_b} \\ &\leq C (d-2) a^{-d+2B^- k_b}. \end{aligned}$$

Here we use the fact that $\tilde{c}\xi_b^{1-d}$ can be bounded by a $\mathcal{O}(1)$ constant C since $1 - d < 0$. Finally, we use that $d - 2$ is small, i.e. that there exists an $\ell > 0$ such that $d - 2 = a^\ell$. If we choose $0 < k_b < (\ell - d - 1)/2|B^-|$, we find that $\phi(\xi_b) \leq Ca$, which completes the proof. The extra condition $\ell > d + 1$ now follows, since k_b must be positive. \square

Remark C.1. The integral $\int_0^{(1/2)T_0^{(k)}} B^{(k)}(s) ds$ can also be approximated using a less precise but easier method as follows. Since $B \geq -1$ for all ξ it can be bounded as $\int_0^{(1/2)T_0^{(k)}} B^{(k)}(s) ds \geq -\frac{1}{2}T_0^{(k)} \geq c|\log a|$ because the period $T_0^{(k)}$ of a solution for $k \rightarrow 1$ is of $\mathcal{O}(|\log a|)$. However, this leads to a less accurate estimate and as a result to a larger lower bound on ℓ .

Remark C.2. A larger range for ℓ can be obtained by relaxing the condition on ϕ to $|\phi| < ca^{1/2}$. With this bound on ϕ , the ϕ^2 term in the B -equation in system (2.8) is still a higher order term compared to the $(a(1 - d)B)/\eta$ term and therefore it is sufficient. This leads to the modified condition $\ell > d + \frac{1}{2}$, where $0 < k_b < (\ell - d - (1/2))/2|B^-|$.

Appendix D. A bound for $(1/A)(dA/d\Delta)$

In this appendix, we derive the bound on $(1/A)(dA/d\Delta)$ that is used in the proof of lemma 10.1. We will use two pieces of information about $A(\xi)$. First, we recall from section 4 that, on the interval $(0, \xi_b)$, $A(\xi)$ is monotonically decreasing. Second, we recall from the previous appendix that, on the interval $[\xi_b, \xi_{\max}]$, $A(\xi)$ is bounded from below,

$$A(\xi) \geq A(\xi_b)a^{1/2} \geq ca^{-B^{-k_b+1/2}}$$

for some $c > 0$. Hence, putting these two pieces of information together, we may conclude that there exists a positive constant c_1 such that, on the full interval $(0, \xi_{\max}]$,

$$\frac{1}{A(\xi)} \leq c_1a^{B^{-k_b-1/2}}.$$

To determine an estimate on $(dA/d\Delta)$, we again use the fact that the constructed solution lies $\mathcal{O}(a)$ close to the heteroclinic orbit of the unperturbed system, (2.8) with $a = 0$. Thus, $A(\xi) = A^{(k)}(\xi) + \mathcal{O}(a)$ for $\xi_b \leq \xi \leq \xi_{\max}$, where $k \rightarrow 1$. Here, $A^{(k)}(\xi)$ does not depend on the dimension d . Hence, $(dA/d\Delta) = \mathcal{O}(a)$. Combining these two estimates, we obtain

$$\frac{1}{A} \frac{dA}{d\Delta} \leq \tilde{c}a^{B^{-k_b+1/2}}$$

for $0 \leq \xi \leq \xi_{\max}$ and a positive constant \tilde{c} .

References

- [1] Abramovitz M and Stegun I A 1972 *Handbook of Mathematical Functions With Formulas, Graphs and Mathematical Tables* (New York: Dover)
- [2] Budd C J 2002 Asymptotics of multi-bump blow-up self-similar solutions of the nonlinear Schrödinger equation *SIAM J. Appl. Math.* **62** 801–30
- [3] Budd C J, Chen S and Russell R D 1999 New self-similar solutions of the nonlinear Schrödinger equation with moving mesh computations *J. Comp. Phys.* **152** 756–89
- [4] Byrd P F and Friedman M D 1954 *Handbook of Elliptic Integrals for Engineers and Physicists* (Berlin, Heidelberg: Springer)
- [5] Cai D, McLaughlin D W and McLaughlin K T R 2002 The nonlinear Schrödinger equation as both a PDE and a dynamical system *Handbook of Dynamical Systems, Towards Applications* vol 2, ed B Fiedler (Amsterdam: North-Holland) pp 599–675
- [6] Chiao R Y, Garmire E and Townes C H 1964 Self-trapping of optical beams *Phys. Rev. Lett.* **13** 479–82
- [7] Coffman C V 1972 Uniqueness of the ground state for $\Delta u - u + u^3 = 0$ and a variational characterization of other solutions *Arch. Ration. Mech. Anal.* **46** 81–95

- [8] Doelman A and Hek G 2000 Homoclinic saddle-node bifurcations in singularly perturbed systems *J. Dyn. Diff. Eqns* **12** 169–216
- [9] Doelman A and Holmes P J 1996 Homoclinic explosions and implosions *Phil. Trans. R. Soc. A* **354** 845–93
- [10] Doelman A and Rottschäfer V 1997 Singularly perturbed and non-local modulation equations for systems with interacting instability mechanisms *J. Nonlinear Sci.* **7** 371–409
- [11] Fenichel N 1979 Geometric singular perturbation theory for ordinary differential equations *J. Diff. Eqns* **31** 53–98
- [12] Fibich G 1996 Adiabatic law for self-focusing of optical beams *Opt. Lett.* **21** 1735–7
- [13] Glassey R T 1977 On the blowing up of the solutions to the Cauchy problem for nonlinear Schrödinger equations *J. Math. Phys.* **18** 1974–7
- [14] Guckenheimer J and Holmes P J 1983 *Nonlinear Oscillations, Dynamical Systems, and Bifurcations of Vector Fields (Applied Mathematical Sciences Series)* vol 42 (New York: Springer)
- [15] Hasegawa A 1989 *Optical Solitons in Fibers* (Berlin: Springer)
- [16] Holmes P, Doelman A, Hek G and Domokos G 2000 Homoclinic orbits and chaos in three- and four-dimensional flows *Phil. Trans. R. Soc. A* **359** 1429–38
- [17] Jones C K R T 1994 Geometric singular perturbation theory *Dynamical Systems, Montecatini Terme (Lecture Notes in Mathematics vol 1609)* ed R Johnson (New York: Springer) pp 44–118
- [18] Jones C K R T, Kaper T J and Kopell N 1996 Tracking invariant manifolds up to exponentially small errors *SIAM J. Math. Anal.* **27** 558–77
- [19] Jones C K R T and Tin S K 2002 Generalized exchange lemmas and orbits heteroclinic to invariant manifolds *Mem. AMS* submitted
- [20] Kaper T J and Jones C K R T 2001 A primer on the Exchange Lemma for fast–slow systems *Multiple-Time-Scale Dynamical Systems (IMA Volumes on Mathematics and its Applications)* vol 122, ed C K R T Jones and A Khibnik (New York: Springer) pp 65–88
- [21] Kaper T J and Kovacic G 1994 A geometric criterion for adiabatic chaos *J. Math. Phys.* **35** 1202–18
- [22] Kaper T J and Kovacic G 1996 Multi-bump orbits homoclinic to resonance bands *Trans. Am. Math. Soc.* **348** 3835–87
- [23] Kopell N and Landman M 1995 Spatial structure of focusing singularity of the nonlinear Schrödinger equation: a geometrical analysis *SIAM J. Appl. Math.* **55** 1297–323
- [24] Kosmatov N E, Shvets V F and Zakharov V E 1991 Computer simulation of wave collapses in the nonlinear Schrödinger equation *Physica D* **52** 16–35
- [25] Landman M J, Papanicolaou G C, Sulem C and Sulem P L 1988 Rate of blowup for solutions of the nonlinear Schrödinger equation at critical dimension *Phys. Rev. A* **38** 3837–43
- [26] Le Mesurier B J, Papanicolaou G C, Sulem C and Sulem P L 1988 Local structure of the self-focusing singularity of the nonlinear Schrödinger equation *Physica D* **32** 210–26
- [27] Le Mesurier B J, Papanicolaou G C, Sulem C and Sulem P L 1986 Focusing and multi-focusing solutions of the nonlinear Schrödinger equation *Physica D* **31** 78–102
- [28] McLaughlin D W, Papanicolaou G C, Sulem C and Sulem P L 1986 The focusing singularity of the cubic Schrödinger equation *Phys. Rev. A* **34** 1200–10
- [29] McLeod K and Serrin J 1981 Uniqueness of solutions of semilinear Poisson equations *Proc. Natl Acad. Sci.* **78** 6592–5
- [30] Neihstadt A I 1975 Passage through a separatrix in a resonance problem with a slowly varying parameter *PMM* **39** 594–605
- [31] Newell A C 1985 *Solitons in Mathematics and Physics (CBMS Applied Mathematical Series)* vol 48 (Philadelphia: SIAM)
- [32] Plecháč P and Šverák V 2001 On self-similar singular solutions of the complex Ginzburg–Landau equation *Commun. Pure Appl. Math.* **54** 1215–42
- [33] Rasmussen J J and Rypdal K 1986 Blowup in nonlinear Schrödinger equations 1. A general review and 2. Similarity structure of the blowup singularity *Phys. Scr.* **33** 481–504
- [34] Robinson C 1983 Sustained resonance for a nonlinear system with slowly varying coefficients *SIAM J. Math. Anal.* **14** 847–960
- [35] Rottschäfer V and Kaper T 2002 Blowup in the nonlinear Schrödinger equation near critical dimension *J. Math. Anal. Appl.* **268** 517–49
- [36] Sulem C and Sulem P L 1999 *The Nonlinear Schrödinger Equation: Self-focusing and Wave Collapse (Applied Mathematical Science Series)* vol 139 (New York: Springer)
- [37] Zakharov V E 1984 Collapse and self-focusing of Langmuir waves *Handbook of Plasma Physics* vol 2 (general) ed M N Rosenbluth and R Z Sagdeev *Basic Plasma Physics II* ed A A Galeev and R N Sudan (Amsterdam: Elsevier) pp 81–121